High Hydride Count Rhodium Octahedra, [Rh$_6$(PR$_3$)$_6$H$_{12}$][BAr$^F_4$]$_2$: Synthesis, Structures, and Reversible Hydrogen Uptake under Mild Conditions

Simon K. Brayshaw,[†] Michael J. Ingleson,[†] Jennifer C. Green,[‡] J. Scott McIndoe,[§]
Paul R. Raithby,[†] Gabriele Kociok-Köhn,[†] and Andrew S. Weller*,[†]

*Contribution from the Departments of Chemistry, University of Bath, Bath BA2 7AY, U.K.,
University of Oxford, Oxford OX1 3QR, U.K., and University of Victoria,
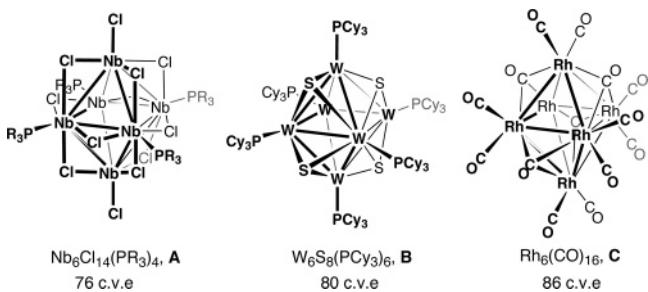Victoria, BC V8W3V6, Canada*

Received January 28, 2006; E-mail: a.s.weller@bath.ac.uk

Abstract: A new class of transition metal cluster is described, [Rh$_6$(PR$_3$)$_6$H$_{12}$][BAr$^F_4$]$_2$ (R = ^{i}Pr (**1a**), Cy (**2a**); BAr$^F_4$ = [B{C$_6$H$_3$(CF$_3$)$_2$}$_4$]$^-$). These clusters are unique in that they have structures exactly like those of early transition metal clusters with edge-bridging π-donor ligands rather than the structures expected for late transition metal clusters with π-acceptor ligands. The solid-state structures of **1a** and **2a** have been determined, and the 12 hydride ligands bridge each Rh–Rh edge of a regular octahedron. Pulsed gradient spin–echo NMR experiments show that the clusters remain intact in solution, having calculated hydrodynamic radii of 9.5(3) Å for **1a** and 10.7(2) Å for **2a**, and the formulation of **1a** and **2a** was unambiguously confirmed by ESI mass spectrometry. Both **1a** and **2a** take up two molecules of H$_2$ to afford the cluster species [Rh$_6$(P^{i}Pr$_3$)$_6$H$_{16}$][BAr$^F_4$]$_2$ (**1b**) and [Rh$_6$(PCy$_3$)$_6$H$_{16}$][BAr$^F_4$]$_2$ (**2b**), respectively, as characterized by NMR spectroscopy, ESI-MS, and, for **2b**, X-ray crystallography using the [1-H-CB$_{11}$Me$_{11}$]$^-$ salt. The hydride ligands were not located by X-ray crystallography, but ^{1}H NMR spectroscopy showed a 15:1 ratio of hydride ligands, suggesting an interstitial hydride ligand. Addition of H$_2$ is reversible: placing **1b** and **2b** under vacuum regenerates **1a** and **2a**. DFT calculations on [Rh$_6$(PH$_3$)$_6$H$_x$]$^{2+}$ (x = 12, 16) support the structural assignments and also show a molecular orbital structure that has 20 orbitals involved with cluster bonding. Cluster formation has been monitored by ^{31}P{^{1}H} and ^{1}H NMR spectroscopy, and mechanisms involving heterolytic H$_2$ cleavage and elimination of [HP^{i}Pr$_3$]$^+$ or the formation of trimetallic intermediates are discussed.

Introduction

The chemistry of transition metal clusters occupies two "classical" areas.[1] The first encompasses clusters with metal atoms in low to medium oxidation states combined with π-donating ligands,[2] exemplified by halide edge-bridged clusters such as [Nb$_6$Cl$_{18}$]K$_4$, Nb$_6$Cl$_{14}$(P^{n}Pr$_3$)$_4$[3] (**A**, Scheme 1), or Zr$_6$-Cl$_{14}$H$_4$(PEt$_3$)$_4$[4] and by the face-bridged chalcogenides [W$_6$S$_8$-(PEt$_3$)$_6$] (**B**)[5] or [Re$_6$Se$_8$I$_6$]$^{4-}$,[6] which are molecular models for Chevrel phases.[7] The second grouping is that of the later transition metals in low oxidation states with π-acceptor ligands such as Rh$_6$(CO)$_{16}$ (**C**) or [Ru$_6$(μ-C)(CO)$_{16}$]$^{2-}$.[8] Aside from the fascinating structural and bonding aspects of these compounds,

Scheme 1. Representative Examples of Octahedral Transition Metal Clusters with π-Donor and π-Acceptor Ligands

Nb$_6$Cl$_{14}$(PR$_3$)$_4$, **A**
76 c.v.e

W$_6$S$_8$(PCy$_3$)$_6$, **B**
80 c.v.e

Rh$_6$(CO)$_{16}$, **C**
86 c.v.e

the driving force for the study of such cluster systems is their potential to bridge the areas of heterogeneous and homogeneous catalysis[1,9,10] and their unique spatial, electronic, and magnetic properties.[11]
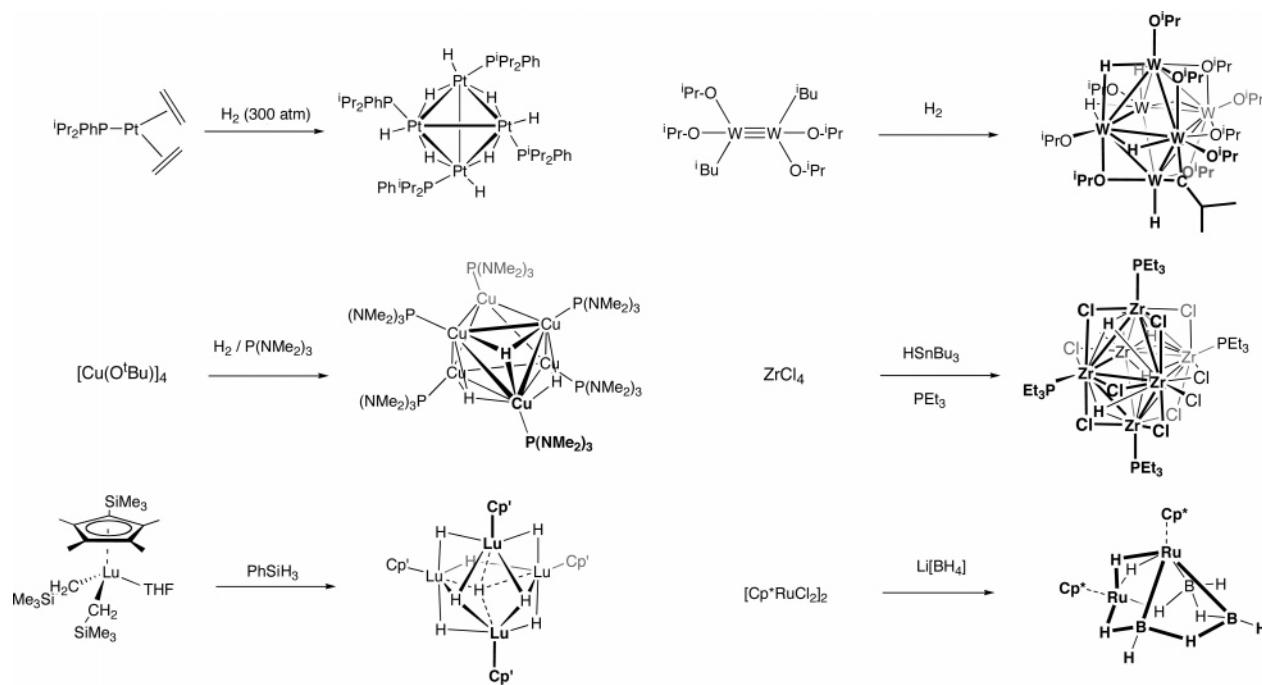
The electronic descriptions for both classes of cluster are well understood, especially for octahedral species where symmetry allows for a concise account of the molecular orbital structures.[12,13] The octahedral late transition metals with π-accepting ligands (**C**) generally have cluster valence electron counts (cve) of 86 electrons,[14] although exceptions do exist.[15] For clusters with π-donor edge-bridging ligands (**A**), electron counts of 74–78 cve have been noted, with 76 cve being usual, while the

[†] University of Bath.
[‡] University of Oxford.
[§] University of Victoria.

(1) *Metal clusters in chemistry*; Braunstein, P., Oro, L. A., Raithby, P. R., Eds.; Wiley-VCH: Weinheim, 1999.
(2) *Early transition metal clusters with π-donor ligands*; Chisholm, M. H., Ed.; VCH: New York, 1995. Gray, T. G. *Coord. Chem. Rev.* **2003**, *243*, 213–235.
(3) Klendworth, D. D.; Walton, R. A. *Inorg. Chem.* **1981**, *20*, 1151–1155.
(4) Chen, L.; Cotton, F. A.; Wojtczak, W. A. *Inorg. Chem.* **1996**, *35*, 2988–2994.
(5) Saito, T. *Adv. Inorg. Chem.* **1997**, *44*, 45–91.
(6) Long, J. R.; McCarty, L. S.; Holm, R. H. *J. Am. Chem. Soc.* **1996**, *118*, 4603–4616.
(7) Chevrel, R.; Sergent, M.; Prigent, J. *J. Solid State Chem.* **1971**, *3*, 515–519.

Scheme 2. Examples of Cluster Buildup under Kinetic Conditions

faced-bridged chalcogenides (**B**) span a larger range of cluster electron counts, from 80 cve in $Mo_6(\mu$-$S)_8(PEt_3)_6$ to 98 cve in $Co_6(\mu$-$S)_8(PEt_3)_6$.[16]
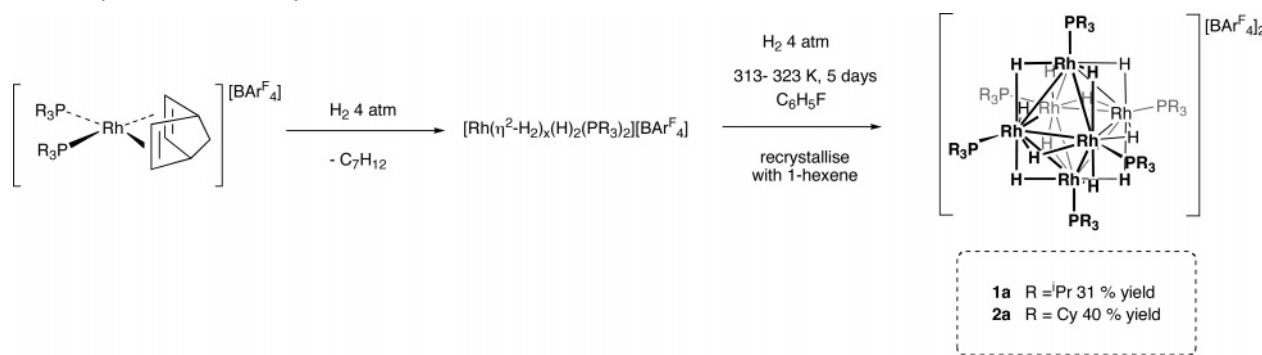
The synthesis of transition metal cluster species from mono- or dinuclear starting materials often favors the isolation of what might be considered the thermodynamic product, by using moderate to high temperature and pressure, or sometimes both.[2,12,17] This invariably leads to products that are electronically and coordinatively saturated, although notable recent examples exist of electronically unsaturated clusters formed from thermolysis reactions when bulky phosphines are used, such as $Pt_3Re_2(CO)_6(P^tBu_3)_3$.[18] Rarer are routes that offer up some degree of kinetic control to cluster formation from mono- or dinuclear precursors, and, relevant to this paper, to our knowledge many of these kinetic routes often result in cluster species with attached hydride ligands, although non-hydride-containing clusters can also be synthesized.[19] Hydrogenolysis of precursor complexes and elimination of non-coordinating alkane or alcohol is a common synthetic method. For example, reaction of $Pt(PR_3)(\eta^2$-$H_2C{=}CH_2)_2$ precursors with H_2 gives platinum hydrido-phosphine clusters such as $Pt_4(P^iPr_2Ph)_4H_8$,[20,21] while addition of H_2 to $(^iPrO)_2(^tBu)W{\equiv}W(^iPrO)_2(^tBu)$ affords $W_6H_5(C^iPr)(O^iPr)_{12}$,[22,23] and reaction of H_2 with $[(^tBuO)Cu]_4$ in the presence of $P(NMe_2)_3$ gives the octahedral copper polyhydride $Cu_6(P(NMe_2)_3)_6H_6$[24] (Scheme 2). An alternative method is to reduce a mononuclear transition metal halide with a hydride source such as $HSnBu_3$ or H_3SiPh to afford compounds such as $Zr_6(PR_3)_4Cl_{14}H_4$[4,25] and $[(\eta^5$-$C_5Me_4SiMe_3)$-$LuH_2]_6$,[26,27] respectively. Kinetic routes to related metallaborane cluster species through reduction of mononuclear cyclopentadienyl halides have also been developed,[28] and hydrido clusters can also be synthesized under kinetic conditions from condensation of bimetallic hydride complexes with monometallic fragments.[29–31]

We report in this paper the synthesis under mild conditions of a new class of octahedral cluster, $[Rh_6(PR_3)_6H_{12}]^{2+}$. Such clusters bridge the gap between early and later transition metals inasmuch as they are composed of *late* transition metal fragments {$Rh(PR_3)$} but have molecular geometries and

(8) Dyson, P. J.; McIndoe, J. S. *Transition metal carbonyl cluster chemistry*; Gordon and Breach Science Publishers: Amsterdam, 2000.
(9) Dumestre, F.; Chaudret, B.; Amiens, C.; Renaud, P.; Fejes, P. *Science* **2004**, *303*, 821–823.
(10) Thomas, J. M.; Johnson, B. F. G.; Raja, R.; Sankar, G.; Midgley, P. A. *Acc. Chem. Res.* **2003**, *36*, 20–30.
(11) Beltran, L. M. C.; Long, J. R. *Acc. Chem. Res.* **2005**, *38*, 325–334. Gabriel, J. C. P.; Boubekeur, K.; Uriel, S.; Batail, P. *Chem. Rev.* **2001**, *101*, 2037–2066.
(12) Mingos, D. M. P.; Wales, D. J. *Introduction to cluster chemistry*; Prentice Hall: London, 1990.
(13) Chisholm, M. H.; Clark, D. L.; Hampdensmith, M. J.; Hoffman, D. H. *Angew. Chem., Int. Ed. Engl.* **1989**, *28*, 432–444.
(14) Mingos, D. M. P. *J. Chem. Soc., Dalton Trans.* **1974**, 133–138.
(15) Paquette, M. S.; Dahl, L. F. *J. Am. Chem. Soc.* **1980**, *102*, 6621–6623.
(16) Lin, Z. Y.; Williams, I. D. *Polyhedron* **1996**, *15*, 3277–3287. Lin, Z. Y.; Fan, M. F. In *Structural and Electronic Paradigms in Cluster Chemistry*; Springer-Verlag: Berlin, 1997; Vol. 87.
(17) *The chemistry of metal cluster complexes*; Shriver, D. F., Kaesz, H. D., Adams, R. D., Eds.; VCH: New York, 1990.
(18) Adams, R. D.; Captain, B. *Angew. Chem., Int. Ed.* **2005**, *44*, 2531–2533.

(19) Adams, R. D.; Captain, B.; Fu, W.; Smith, M. D. *J. Am. Chem. Soc.* **2002**, *124*, 5628–5629. Adams, R. D.; Captain, B.; Fu, W.; Hall, M. B.; Manson, J.; Smith, M. D.; Webster, C. E. *J. Am. Chem. Soc.* **2004**, *126*, 5253–5267. Stone, F. G. A. *Pure Appl. Chem.* **1986**, *58*, 529–536. Stone, F. G. A. *Angew. Chem., Int. Ed. Engl.* **1984**, *23*, 89–99.
(20) Gregson, D.; Howard, J. A. K.; Murray, M.; Spencer, J. L. *J. Chem. Soc., Chem. Commun.* **1981**, 716–717.
(21) Frost, P. W.; Howard, J. A. K.; Spencer, J. L.; Turner, D. G.; Gregson, D. *J. Chem. Soc., Chem. Commun.* **1981**, 1104–1106.
(22) Chisholm, M. H.; Folting, K.; Kramer, K. S.; Streib, W. E. *J. Am. Chem. Soc.* **1997**, *119*, 5528–5539.
(23) Chisholm, M. H.; Kramer, K. S. *Chem. Commun.* **1996**, 1331–1332.
(24) Lemmen, T. H.; Folting, K.; Huffman, J. C.; Caulton, K. G. *J. Am. Chem. Soc.* **1985**, *107*, 7774–7775.
(25) Chen, L. F.; Cotton, F. A. *Inorg. Chim. Acta* **1997**, *257*, 105–120.
(26) Tardif, O.; Nishiura, M.; Hou, Z. M. *Organometallics* **2003**, *22*, 1171–1173.
(27) Cui, D. M.; Tardif, O.; Hou, Z. M. *J. Am. Chem. Soc.* **2004**, *126*, 1312–1313. Luo, Y.; Baldamus, J.; Tardif, O.; Hou, Z. M. *Organometallics* **2005**, *24*, 4362–4366.
(28) Fehlner, T. P. *Organometallics* **2000**, *19*, 2643–2651.
(29) Rhodes, L. F.; Huffman, J. C.; Caulton, K. G. *J. Am. Chem. Soc.* **1983**, *105*, 5137–5138.
(30) Suzuki, H.; Kakigano, T.; Tada, K.; Igarashi, M.; Matsubara, K.; Inagaki, A.; Oshima, M.; Takao, T. *Bull. Chem. Soc. Jpn.* **2005**, *78*, 67–87.
(31) Vieille-Petit, L.; Tschan, M. J. L.; Suss-Fink, G.; Laurenczy, G.; Hagen, C. M.; Finke, R. G.; Geneste, F.; Moinet, C. *Polyhedron* **2005**, *24*, 1961–1967.

Scheme 3. Synthesis of the 12-Hydride Clusters **1a** and **2a**

electronic structures that are more closely related to those of the *early* octahedral transition metal clusters. Not only do these clusters have unprecedented structures for a late transition metal cluster species but they also have an extraordinarily large number of hydride ligands associated with them and thus are potential models for nanoparticle Rh clusters used in arene hydrogenations,[10,32] hydrogen storage materials,[33−35] and hydrogen spillover systems.[36] We demonstrate their relevance to these areas by describing the facile and reversible dihydrogen uptake by these clusters under very mild conditions of room temperature and pressure. The structures of these new cluster species have been probed by a combination of X-ray crystallography, NMR spectroscopy, electrospray ionization mass spectrometry, and DFT calculations, and we also report on studies to elucidate the mechanism of cluster formation from mononuclear rhodium precursor complexes. Aspects of this work have been communicated previously.[37,38]

Results and Discussion

Synthesis and Solid-State Structure of $[Rh_6(PR_3)_6H_{12}]$-$[BAr^F_4]_2$ (R = ^{i}Pr, Cy). We have recently reported that addition of H_2 (∼4 atm initially, 298 K) to CH_2Cl_2 or fluorobenzene solutions of $[Rh(PR_3)_2(nbd)][BAr^F_4]$ (R = ^{i}Pr, Cy; BAr^F_4 = $[B\{C_6H_3(CF_3)_2\}_4]^-$, nbd = norbornadiene) initially results in the formation of the almost colorless dihydrogen/dihydride complexes $[Rh(PR_3)_2(H)_2(\eta^2-H_2)_x][BAr^F_4]$ (x = 1 or 2).[39] Gentle heating (313−323 K) of these solutions results in a gradual darkening to very dark red over 4 days and the formation of the dicationic octahedral cluster species $[Rh_6(PR_3)_6H_{12}][BAr^F_4]_2$, isolated in moderate yield as analytically pure salts on recrystallization (**1a**, R = ^{i}Pr, 31%; **2a**, R = Cy, 40% yield, based on rhodium). Recrystallization from solutions containing an excess of 1-hexene ensures the isolation of the 12-hydride species and not clusters with a higher hydride count (16 hydrides), which can form readily on exposure of **1a** or **2a** to H_2 present in the reaction vessel (vide infra). The mechanism of cluster formation and hydrogen uptake experiments will be discussed in due course, and we first present the complete characterization of clusters **1a** and **2a** by X-ray crystallography, NMR spectroscopy, and mass spectrometry. Using CH_2Cl_2 as the reaction solvent rather than fluorobenzene resulted in lower yields of cluster, and thus the latter is preferred. Anions other than $[BAr^F_4]^-$ gave mixed results. Use of the "greasy ball" weakly coordinating

anion $[1\text{-}closo\text{-}HCB_{11}Me_{11}]^{-\ 40}$ afforded clusters in effectively the same yield as for $[BAr^F_4]^-$, but $[PF_6]^-$ or $[BF_4]^-$ resulted in no cluster formation, principally because these latter two anions are not compatible with the formation of the intermediate dihydrogen complexes (Scheme 3). Compound **1a** is sparingly soluble in fluorobenzene (marginally better in CH_2Cl_2), while **2a** shows better solubility in either solvent. They are both insoluble in pentane and toluene.

The solid-state structures of the triisopropylphosphine cluster **1a** and the tricyclohexylphosphine cluster **2a** are shown in Figure 1. Table 1 gives data collection and refinement details, and Table 2 presents a comparison of the key structural metrics of these clusters. Full listings of bond lengths and angles are given in the Supporting Information. **1a** has a crystallographically imposed centrosymmetric structure in the solid state, while **2a** does not, but both are effectively regular Rh_6 octahedra. Each rhodium vertex is coordinated with a single phosphine, which is directed approximately radial to the cluster core, with the cross-cluster Rh···Rh−P angles, e.g. Rh(2′)···Rh(2)−P(2) in **1a**, being only a few degrees away from 180° (average 176.6-(1) and 177.8(1)° for **1a** and **2a**, respectively). The Rh−Rh distances are only slightly larger for **2a** than measured for **1a** (averages for **1a**, 2.720 Å; for **2a**, 2.735 Å), and there is only a slight increase in cross-cluster P···P distances, showing that the bulkier tricyclohexylphosphine ligands (cone angle for PCy_3 is 169° vs 159° for P^iPr_3[41]) have only a small effect on the cluster geometry. The deviation of Rh−Rh bonding distances, δ(Rh−Rh), is essentially the same for both and is small (∼0.03 Å), as is deviation in cross-cluster Rh−Rh distances. DiSalvo

(32) Dyson, P. J. *Dalton Trans.* **2003**, 2964−2974. Hagen, C. M.; Vieille-Petit, L.; Laurenczy, G.; Suss-Fink, G.; Finke, R. G. *Organometallics* **2005**, *24*, 1819−1831. Hagen, C. M.; Widegren, J. A.; Maitlis, P. M.; Finke, R. G. *J. Am. Chem. Soc.* **2005**, *127*, 4423−4432.

(33) Schlapbach, L.; Zuttel, A. *Nature* **2001**, *414*, 353−358.

(34) Rowsell, J. L. C.; Eckert, J.; Yaghi, O. M. *J. Am. Chem. Soc.* **2005**, *127*, 14904−14910. Rowsell, J. L. C.; Spencer, E. C.; Eckert, J.; Howard, J. A. K.; Yaghi, O. M. *Science* **2005**, *309*, 1350−1354. Rowsell, J. L. C.; Yaghi, O. M. *Angew. Chem., Int. Ed.* **2005**, *44*, 4670−4679.

(35) Dinca, M.; Long, J. R. *J. Am. Chem. Soc.* **2005**, *127*, 9376−9377. Kaye, S. S.; Long, J. R. *J. Am. Chem. Soc.* **2005**, *127*, 6506−6507.

(36) Gao, H. R.; Angelici, R. J. *J. Am. Chem. Soc.* **1997**, *119*, 6937−6938. Conner, W. C.; Falconer, J. L. *Chem. Rev.* **1995**, *95*, 759−788. Lachawiec, A. J.; Qi, G. S.; Yang, R. T. *Langmuir* **2005**, *21*, 11418−11424.

(37) Brayshaw, S. K.; Ingleson, M. J.; Green, J. C.; Raithby, P. R.; Kociok-Kohn, G.; McIndoe, J. S.; Weller, A. S. *Angew. Chem., Int. Ed.* **2005**, *44*, 6875−6878.

(38) Ingleson, M. J.; Mahon, M. F.; Raithby, P. R.; Weller, A. S. *J. Am. Chem. Soc.* **2004**, *126*, 4784−4785.

(39) Ingleson, M. J.; Brayshaw, S. K.; Mahon, M. F.; Ruggiero, G. D.; Weller, A. S. *Inorg. Chem.* **2005**, *44*, 3162−3171.

(40) King, B. T.; Janousek, Z.; Gruner, B.; Trammell, M.; Noll, B. C.; Michl, J. *J. Am. Chem. Soc.* **1996**, *118*, 3313−3314. Clarke, A. J.; Ingleson, M. J.; Kociok-Kohn, G.; Mahon, M. F.; Patmore, N. J.; Rourke, J. P.; Ruggiero, G. D.; Weller, A. S. *J. Am. Chem. Soc.* **2004**, *126*, 1503−1517.

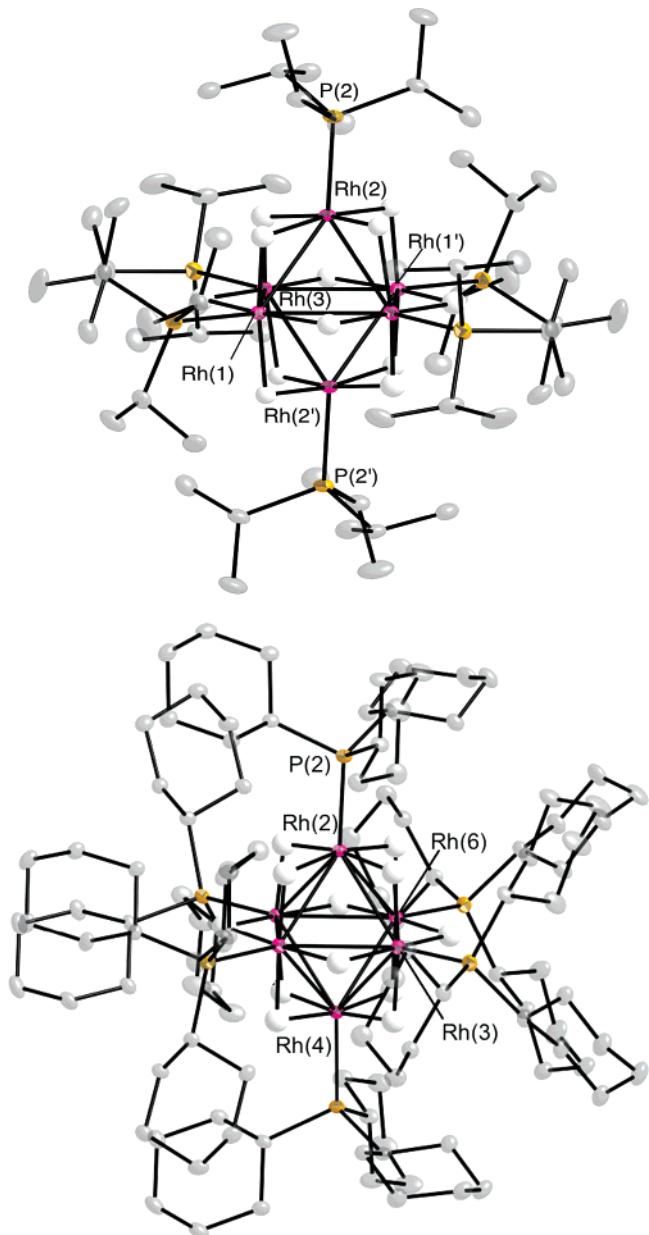(41) Tolman, C. A. *Chem. Rev.* **1977**, *77*, 313−348.

Figure 1. Solid-state structure of the dications in **1a** (top) and **2a** (bottom). Thermal ellipsoids are shown at the 50% probability level. The counterions are not shown. Apart from the hydride ligands, all other hydrogen atoms have been omitted for clarity.

and co-workers have noted similar small changes to the cluster core on going from PEt_3 to the bulkier PCy_3 in the octahedral face-bridged sufide clusters $W_6S_8(PR_3)_6$.[42] The direct Rh–Rh distances in **1a** and **2a** are also comparable to those found in $Rh_6(CO)_{16}$ (average 2.750 Å).[43]

For both **1a** and **2a**, the 12 hydride ligands were located in the final difference map, and each Rh–Rh edge in the respective octahedra is spanned by a bridging hydride ligand, forming a cuboctahedron surrounding the metal core (Figure 2 shows **1a**). Three independently synthesized samples of **1a** gave similar high-quality data and are all in agreement with the gross positioning of the hydride ligands over Rh–Rh edges. The

location of hydride ligands in transition metal clusters by X-ray crystallography is often problematic, given the low scattering associated with the M–H bond, but, as will be reported later, NMR, mass spectral, and microanalysis data all unequivocally support the formulation as 12-hydride clusters for both **1a** and **2a**. Comparison of the Rh–H distances in **1a** suggests that, within error, six of these hydrides are more semi-bridging than bridging in nature, although the difference between the two modes is rather subtle, especially as measured by X-ray crystallography. DFT calculations (vide infra) also suggest a mixture of bridging and semi-bridging hydrides, with four octahedral edges bridged symmetrically and the remaining eight bridged unsymmetrically, supporting such a structural assignment. Of course, a neutron diffraction study would help pin down the positioning of the hydrides, as it has for cluster hydride ligands previously,[44–47] and attempts are currently underway to produce crystals of a size suitable for such an experiment.

Transition metal clusters with hydride ligands are ubiquitous.[1,8,12,17] However, those with more than four hydride ligands, or a hydride:metal ratio of >1, are significantly less well documented. Well-characterized examples of clusters with a high (>4) hydride count include $Pt_5H_8(P^tBu_2Ph)_5$,[20] $[Pt_4H_7(P^tBu_3)_4]$-$[BF_4]$,[48] $Pt_2Os_7(CO)_{23}H_8$,[49] $[Zr_6Cl_{18}H_5][PPh_4]_3$,[47] $Cu_6(PR_6)_6H_6$,[24] $Pd_{28}(PtPMe_3)(PtPPh_3)_{12}(CO)_{27}H_{12}$,[50] $[\{Ru(\eta^6\text{-}C_6H_6)\}_4H_6]Cl_2$,[51] $Os_5Pd(CO)_{16}H_6$,[52] $(Cp^*Ru)_3H_5$,[30] $Os_7Rh_3(CO)_{23}H_{11}$,[53] $OsPt_3$-$Re_2(CO)_6(P^tBu_3)_3H_6$,[18] $[(\eta^5\text{-}C_5Me_4SiMe_3)LuH_2]_6$,[26] $[Re_4Cu_2H_{16}$-$(PMe_2Ph)_8][PF_6]$,[29] and $[Ir_3(L)_3(L')_3H_7][PF_6]_2$ (L = PCy_3, L' = py;[54] L = L' = $PHOX^{55}$). In particular, the edge-bridging arrangement of the hydride ligands in **1a** and **2a** is reminiscent of that observed in octahedral $W_6(C^iPr)(O^iPr)_{12}H_5$,[22] while the simple stoichiometry of $\{Rh(PR_3)H_2\}$ is similar to that of the hydrido-platinum monophosphine clusters such as $Pt_4(P^iPr_2\text{-}Ph)_4H_8$ (Scheme 2).[21] There is also a marked structural similarity between the arrangement of hydride ligands and the positioning of edge-bridging chlorides in the early transition metal clusters (Figure 1), such as $[NbCl_{18}]^{2-}$[3] or $Zr_6Cl_{12}H_2(PEt_3)_6$[25] and especially $Zr_6Cl_{12}(PMe_2Ph)_6$.[56] This structural motif is unknown in the chemistry of rhodium clusters, which is dominated by complexes with carbonyl ligands and $\{Rh(CO)_3\}$ fragments, although a small number of non-carbonyl bi- and trimetallic hydrido-phosphine species with bridging hydride ligands have been reported, such as $[Rh\{P(OR)_3\}_2H]_3$[57,58] and $[Rh_2H_5(P^i\text{-}Pr_3)_4]^+$.[59]

(42) Jin, S.; Venkataraman, D.; DiSalvo, F. J. *Inorg. Chem.* **2000**, *39*, 2747–2757.

(43) Farrar, D. H.; Grachova, E. V.; Lough, A.; Patirana, C.; Poe, A. J.; Tunik, S. P. *J. Chem. Soc., Dalton Trans.* **2001**, 2015–2019.

(44) Bau, R.; Ho, N. N.; Schneider, J. J.; Mason, S. A.; McIntyre, G. J. *Inorg. Chem.* **2004**, *43*, 555–558.

(45) Jackson, P. F.; Johnson, B. F. G.; Lewis, J.; Raithby, P. R.; McPartlin, M.; Nelson, W. J. H.; Rouse, K. D.; Allibon, J.; Mason, S. A. *J. Chem. Soc., Chem. Commun.* **1980**, 295–297.

(46) Hart, D. W.; Teller, R. G.; Wei, C. Y.; Bau, R.; Longoni, G.; Campanella, S.; Chini, P.; Koetzle, T. F. *J. Am. Chem. Soc.* **1981**, *103*, 1458–1466.

(47) Chen, L. F.; Cotton, F. A.; Klooster, W. T.; Koetzle, T. F. *J. Am. Chem. Soc.* **1997**, *119*, 12175–12183.

(48) Goodfellow, R. J.; Hamon, E. M.; Howard, J. A. K.; Spencer, J. L.; Turner, D. G. *J. Chem. Soc., Chem. Commun.* **1984**, 1604–1606.

(49) Adams, R. D.; Pompeo, M. P.; Wu, W. G. *Inorg. Chem.* **1991**, *30*, 2899–2905.

(50) Bemis, J. M.; Dahl, L. F. *J. Am. Chem. Soc.* **1997**, *119*, 4545–4546.

(51) Suss-Fink, G.; Plasseraud, L.; Maisse-Francois, A.; Stoeckli-Evans, H.; Berke, H.; Fox, T.; Gautier, R.; Saillard, J. Y. *J. Organomet. Chem.* **2000**, *609*, 196–203.

(52) Chan, S.; Wong, W. T. *J. Chem. Soc., Dalton Trans.* **1995**, 3987–3994.

(53) Lau, J. P. K.; Wong, W. T. *Dalton Trans.* **2005**, 2579–2587.

(54) Chodosh, D. F.; Crabtree, R. H.; Felkin, H.; Morehouse, S.; Morris, G. E. *Inorg. Chem.* **1982**, *21*, 1307–1311.

(55) Smidt, S. P.; Pfaltz, A.; Martinez-Viviente, E.; Pregosin, P. S.; Albinati, A. *Organometallics* **2003**, *22*, 1000–1009.

(56) Cotton, F. A.; Kibala, P. A.; Roth, W. J. *J. Am. Chem. Soc.* **1988**, *110*, 298–300.

Table 1. Crystal and Structure Refinement Data for the New Cluster Compounds

	compound		
	1a[BArF$_4$]$_2$·(C$_6$H$_5$F)	**2a**[BArF$_4$]$_2$·(C$_7$H$_8$)·(CH$_2$Cl$_2$)$_{2.63}$	**2b**[HCB$_{11}$Me$_{11}$]$_2$·CH$_2$Cl$_2$
empirical formula	C$_{124}$H$_{166}$B$_2$F$_{49}$P$_6$Rh$_6$	C$_{181.63}$H$_{247.25}$B$_2$F$_{48}$P$_6$Rh$_6$Cl$_{5.25}$	C$_{133}$H$_{271}$B$_{22}$Cl$_2$P$_6$Rh$_6$
formula weight	3412.47	4353.56	2982.50
temperature, K	150(2)	150(2)	150(2)
wavelength, Å	0.71073	0.71073	0.71073
crystal system	triclinic	monoclinic	orthorhombic
space group	$P\bar{1}$	$C2/c$	$Pca2_1$
a, Å	13.3466(1)	69.5388(4)	17.6720(2)
b, Å	17.3989(2)	20.4464(1)	28.0280(3)
c, Å	17.8425(1)	27.8999(2	31.0780(5)
α, °	73.208(4)	90	90
β, °	68.263(4)	100.821(1)	90
γ, °	88.452(3)	90	90
volume/Å^3	3669.66(5)	38963.2(4)	15393.3(3)
Z	1	8	4
density (calcd), mg/m^3	1.544	1.484	1.287
absorption coefficient, mm^{-1}	0.830	0.712	0.769
$F(000)$	1721	17826	6292
crystal size, mm	0.35 × 0.15 × 0.10	0.40 × 0.40 × 0.10	0.25 × 0.13 × 0.08
θ range for data collection, °	3.08 to 28.31	3.54 to 30.07	3.55 to 27.10
reflections collected	68058	286379	64581
independent reflections	17997 [R(int) = 0.0433]	56646 [R(int) = 0.0601]	27469 [R(int) = 0.0614]
data/restraints/parameters	17997/0/980	56646/12/2347	27469/1/1535
largest diff peak and hole, e/Å^3	0.788 and −0.775	2.533 and −1.157	1.136 and −1.106
final $R^{a,b}$ indices [$I > 2\sigma(I)$]	$R_1 = 0.0319$	$R_1 = 0.0509$	$R_1 = 0.0561$
	w$R_2 = 0.0739$	w$R_2 = 0.1188$	w$R_2 = 0.1105$
$R^{a,b}$ indices (all data)	$R_1 = 0.0398$	$R_1 = 0.1050$	$R_1 = 0.0940$
	w$R_2 = 0.0770$	w$R_2 = 0.1452$	w$R_2 = 0.1216$
goodness-of-fit on $F^{2\ c}$	1.025	1.022	1.028

^{a} $R_1 = \Sigma||F_o| - |F_c||/\Sigma|F_o|$. ^{b} w$R_2 = \{\Sigma[w(F_o^2 - F_c^2)^2]/\Sigma[w(F_o^2)^2]\}^{1/2}$. ^{c} GOF = S = $\{\Sigma[w(F_o^2 - F_c^2)^2]/(n - p)\}^{1/2}$.

Table 2. Selected Interatomic Distances (Å) for the Crystallographically and Theoretically (ADF, TZVP) Determined 12- and 16-Hydride Clusters

	1a[BArF$_4$]$_2$ H$_{12}$-P^{i}Pr$_3$	**2a**[BArF$_4$]$_2$ H$_{12}$-PCy$_3$	**2b**[HCB$_{11}$Me$_{11}$]$_2$ H$_{16}$-PCy$_3$	[Rh$_6$(PH$_3$)$_6$H$_{12}$]$^{2+}$ calculated	[Rh$_6$(PH$_3$)$_6$H$_{16}$]$^{2+}$ calculated
Rh−Rh mean, Å	2.720	2.735	2.815	2.708	2.789
Rh−Rh, Å	2.700(1)−2.733(1)	2.719(1)−2.743(1)	2.720(1)−3.132(1)	2.667−2.747	2.642−3.017
δ(Rh−Rh), Å^a	0.033	0.024	0.412	0.080	0.375
Rh···Rh cross-cluster, Å	3.825(1)−3.863(1)	3.858(1)−3.869(1)	3.840(1)−4.063(1)	3.795−3.866	3.718−4.124
δ(Rh···Rh), Å	0.038	0.011	0.223	0.071	0.406
P···P cross-cluster, Å	8.313(1)−8.351(1)	8.379−8.392	8.131(2)−8.519(2)	8.219−8.266	8.016−8.385
δ(P···P), Å^a	0.038	0.013	0.388	0.047	0.369
Rh−P, Å	2.246(1)−2.247(1)	2.260(1)−2.264(1)	2.235(2)−2.271(2)	2.203−2.220	2.209−2.227
δ(Rh−P), Å	0.001	0.004	0.036	0.017	0.018
Rh−P mean, Å	2.246	2.262	2.252	2.212	2.218
Rh···Rh−P, deg	176.2(1)−177.2(1)	177.3(1)−178.3(1)	166.8(1)−177.1(1)	172.5−176.5	153.2−174.2
δ(Rh···Rh−P), deg	1.0	1.0	10.3	4.0	21.0

^{a} Maximum deviation in distances. ^{b} Calculated assuming a regular octahedron using the mean Rh−Rh distance.

The cluster cores in both **1a** and **2a** are surrounded by an alkyl sheath formed by the phosphine ligands, presenting a nonpolar outer layer, shielding the inner {Rh$_6$P$_6$H$_{12}$}$^{2+}$ core (Figure 3). For **1a**, the ^{i}Pr$_3$P ligands appear to pack so as to allow more appreciable gaps in the alkyl sheath, whereas in **2a** the cyclohexyl groups shroud the core more effectively. It is remarkable that, especially for the tricyclohexyl phosphines in **2a**, enough space can be found to accommodate six ligands, and the interdigitation of the cyclohexyl groups clearly occurs effectively. Similar packing of cyclohexyl groups has been observed in the closely related cluster W$_6$S$_8$(PCy$_3$)$_6$.[42] The two clusters have appreciable van der Waals diameters of 1.6 nm (**1a**) and 1.8 nm (**2a**). With reference to the unusual electronic
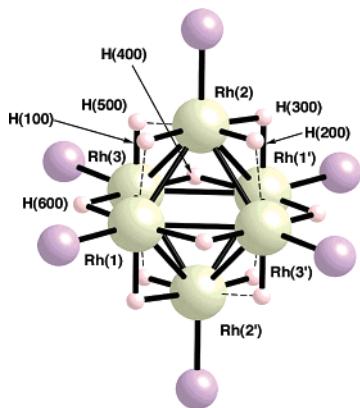
structure of these clusters, this protective cover may well be the reason why they can be isolated.

Solution NMR and Mass Spectrometric Characterization of 1a and 2a. Complex **1a** shows lower solubility in CH$_2$Cl$_2$ solution than **2a**, which is readily soluble (>40 mg/cm^3). Although **1a** will dissolve in CH$_2$Cl$_2$ (~10 mg/cm^3) on sonication for 10 min, overnight it tends to recrystallize, even from CH$_2$Cl$_2$ solutions. Nevertheless, the solubility is more than adequate for the acquisition of good room-temperature solution NMR data. Both complexes are stable in CD$_2$Cl$_2$ solutions for weeks under rigorous exclusion of air and moisture. The ^{31}P-{^{1}H} NMR spectrum of **1a** shows a single, sharp peak centered at δ 106.2 ppm which shows coupling to ^{103}Rh [J(RhP) = 104 Hz]. For **2a**, a broadened doublet is observed at δ 91.9 ppm [J(RhP) = 103 Hz]. In its ^{1}H NMR spectrum, **1a** shows signals due to [BArF$_4$]$^-$ and ^{i}Pr$_3$ groups in the correct ratio for a dicationic cluster. The high-field region displays a single, rather

(57) Brown, R. K.; Williams, J. M.; Sivak, A. J.; Muetterties, E. L. *Inorg. Chem.* **1980**, *19*, 370−374.
(58) Sivak, A. J.; Muetterties, E. L. *J. Am. Chem. Soc.* **1979**, *101*, 4878−4887.
(59) Wolf, J.; Nurnberg, O.; Schafer, M.; Werner, H. *Z. Anorg. Allg. Chem.* **1994**, *620*, 1157−1162.

	Rh–H / Å	Rh–H / Å
H(100)	1.70(3)	1.90(3)
H(200)	1.63(3)	1.96(3)
H(300)	1.78(3)	1.85(3)
H(400)	1.73(3)	1.88(3)
H(500)	1.58(3)	1.93(3)
H(600)	1.72(3)	1.86(3)

Figure 2. Solid-state structure of cationic cluster **1a** showing the cluster core (phosphine alkyl groups have been omitted for clarity). Inset shows selected Rh–H bond distances (Å).
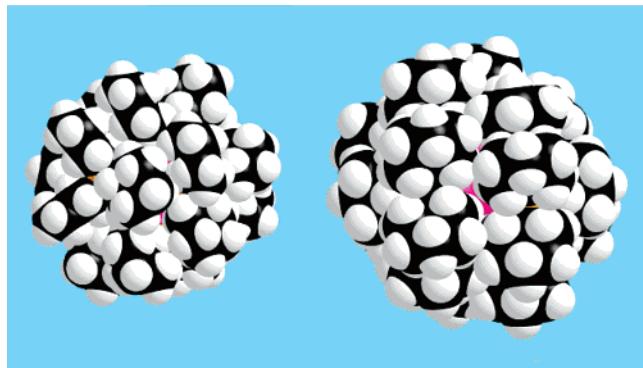

Figure 3. Space-filling diagrams of the cationic portions of **1a** (left) and **2a** (right). Atoms are shown at their respective van der Waals radii. The approximate diameter of these molecules in the solid-state is 1.6 and 1.8 nm, respectively.

broad resonance at δ −25.44 ppm (fwhm = 46 Hz) that integrates to 12 H relative to both the ^{i}Pr protons and the [BAr$^F_4$]$^-$ aromatic protons. Correct integration of hydride signals can often be problematic due to slow relaxation, and long delays between pulses (5 s) and a large number of scans were used to ensure that the true integral value was obtained. Average integral values over at least three samples were also taken, with individual integrals between each sample deviating by less than ±0.5 H. No fine structure to this hydride signal was observed, and decoupling ^{31}P did not narrow the signal significantly or reveal any coupling to ^{103}Rh, which was unfortunate as ^{1}H-{^{31}P} NMR spectra are potentially useful in confirming the number of rhodium atoms with which each hydride environment couples.[58] Cooling to 200 K broadens the hydride peak significantly and shifts it downfield by ca. 5 ppm to δ −19.0 ppm. This might be indicative of a fluxional process, possibly restricted rotation of the phosphine (see later), but the low solubility of **1a** could also contribute to a poorly resolved peak
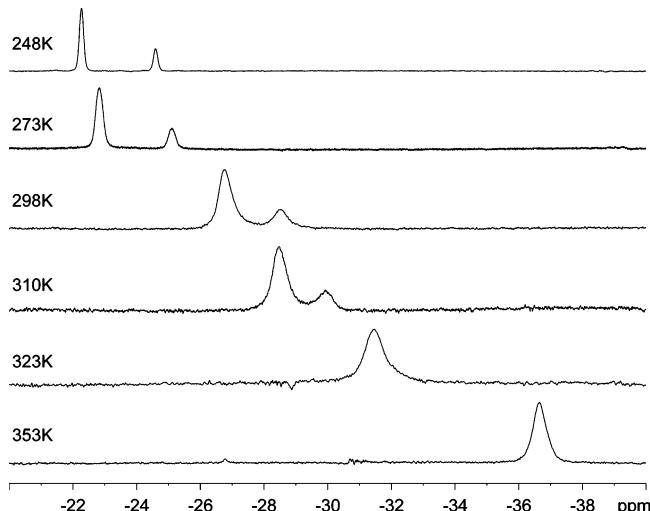

Figure 4. Variable temperature ^{1}H NMR spectrum of **2a** between 248 and 353 K, showing the high-field region (1,2-C$_6$H$_4$F$_2$ solution).

at low temperature. At temperatures higher than 320 K, complex **1a** starts to decompose (C$_6$H$_4$F$_2$ solution). The room-temperature ^{13}C{^{1}H} NMR spectrum shows only two signals for the ^{i}Pr groups, which demonstrates that the phosphine ligands rotate (or at least librate) around their Rh–P axes at room temperature. A low-temperature spectrum was not possible to acquire due to the low solubility of **1a**.

The room-temperature ^{1}H NMR spectrum of **2a**, unlike that of **1a**, displays *two* broad high-field peaks that consistently integrate in the ratio 9 H:3 H with respect to the other signals in the spectrum, at δ −27.0 ppm (fwhm = 230 Hz) and δ −28.9 ppm (fwhm = 330 Hz), respectively. The signals are invariant in ratio on slow cooling to 200 K, suggesting that they are not due to two species in dynamic equilibrium. They do sharpen significantly at the lower temperature and (as for **1a**) shift to lower field (δ −21.7 and −25.2 ppm, respectively at 248 K). At higher temperatures these signals coalesce and then become a single peak (at 353 K) shifted upfield to δ −36.8 ppm, which integrates to 12.2 H (Figure 4). The ^{31}P{^{1}H} NMR spectra show one phosphorus peak over all temperature ranges that also sharpens on cooling and shifts appreciably upfield by $\Delta\delta$ −12 ppm. Although there are a number of possible reasons for the observation of two signals at low temperature (e.g., an alternative trigonal-prismatic structure, or a mixture of bridging and terminal hydrides), we favor the simple explanation of restricted rotation of the bulky tricyclohexyl phosphine groups at or below room temperature. This contrasts with triisopropyl phosphine ligands in **1a**. This restricted rotation leads to hydride ligands that either lie directly under a cyclohexyl group or between two cyclohexyl groups, which results in different bridging hydride environments (Figure 5). Close inspection of the solid-state structure of **2a** reveals three such environments, in the ratio 6:3:3, consistent with the 9:3 pattern observed in solution by ^{1}H NMR spectroscopy. The observation of different hydride environments also shows that the hydrides are not fluxional over the surface of the cluster at low temperature. A ^{13}C{^{1}H} NMR spectrum of **2a** at 250 K (see Supporting Information) shows 15 cyclohexyl environments (some representing coincident peaks), consistent with restricted rotation of the phosphine ligand. These signals broaden on warming, but decomposition at higher temperatures (350 K) prevented the acquisition of a
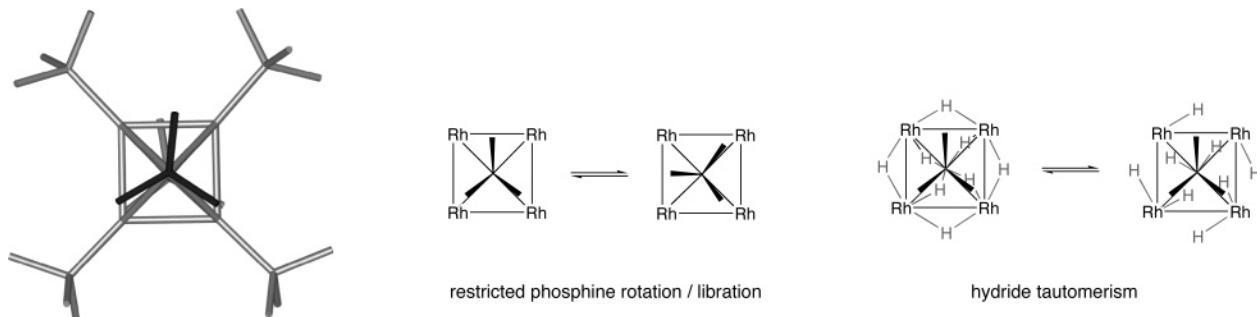
Figure 5. Stick representation of the cluster core in **2a** and the two postulated fluxional processes occurring in **1a/2a**. Cyclohexyl groups apart from the ipso-carbon have been removed to more clearly demonstrate the alignment of the tricyclohexylphosphine ligands.

meaningful $^{13}C\{^1H\}$ NMR spectrum at the high temperature limit. A freely rotating ligand set would be expected to show only six separate environments for the PCy_3 ligands in the ^{13}C-$\{^1H\}$ NMR spectrum, while a static ligand set would give 18. The gradual upfield shift of the hydride signal on warming from 200 to 353 K suggests a rapid, temperature-dependent equilibrium between two Rh–H environments (e.g., a bridging vs terminal tautomerism), one of which is favored at high temperature. Involvement of solvent at higher temperatures is discounted, as the same spectral changes are observed in CD_2-Cl_2, fluorobenzene, or 1,2-difluorobenzene solutions.

At 200 K, the longitudinal relaxation time of the hydrogen ligands on the clusters (T_1)[60,61] is measured as 320 ms for **1a** and 890 ms for each resonance in **2a**, firmly in the region associated with hydride and not dihydrogen ligands, consistent with both the X-ray structures and the structure calculated by DFT (vide infra). For comparison, the bridging hydrides in Ir_4H_4-$(\mu$-H$)_4(CO)_4(PPh_3)_4$ have a T_1 of 690 to 290 ms,[62] while in $[Ru_4H_6(C_6H_6)_4]^{2+}$ the bridging hydrides have T_1 of between 190 and 310 ms.[51] This latter complex is also suggested to have a cluster dihydrogen ligand on the basis of a short $(T_1 = 34$ ms$)$ relaxation time at 153 K.

The structure of the clusters in solution has also been probed using pulsed gradient spin–echo (PGSE) NMR experiments. Such experiments have been used to measure the size of molecules in solution by their calculated hydrodynamic radii.[63,64] A PGSE experiment on **1a** in CD_2Cl_2 solution afforded a hydrodynamic radius (r_H) of 9.5(3) Å for the dication. As expected for the tricyclohexyl phosphine cluster **2a**, a slightly larger r_H value is calculated, 10.7(2) Å (Figure 6). These values are both slightly larger than those measured in the solid state (8.0 and 9.0 Å, respectively). The $[BAr^F_4]^-$ anions in each $(r_H = 7.8(2)$ Å) are also slightly larger in solution than found in the solid state (7.2 Å). These increases in calculated radii are suggestive of ion-pairing between the anions and dication in solution, a not-uncommon feature of ion-pairs in CH_2Cl_2 solution.[63] What these values confirm is that, in solution, the clusters are intact and do not dissociate appreciably into mononuclear solvent-stabilized fragments, e.g., $[Rh(PR_3)(H)_2$-$(solvent)_x][BAr^F_4]$, on the NMR time scale, as these would be

(60) Crabtree, R. H.; Lavin, M. *J. Chem. Soc., Chem. Commun.* **1985**, 1661–1662. Crabtree, R. H. *Acc. Chem. Res.* **1990**, *23*, 95.
(61) Kubas, G. J. *Metal Dihydrogen and σ-Bond Complexes*; Kluwer Academic/Plenum Publishers: New York, 2001.
(62) Garlaschelli, L.; Greco, F.; Peli, G.; Manassero, M.; Sansoni, M.; Gobetto, R.; Salassa, L.; Della Pergola, R. *Eur. J. Inorg. Chem.* **2003**, 2108–2112.
(63) Pregosin, P. S.; Kumar, P. G. A.; Fernandez, I. *Chem. Rev.* **2005**, *105*, 2977–2998.
(64) Pregosin, P. S.; Martinez-Viviente, E.; Kumar, P. G. A. *Dalton Trans.* **2003**, 4007–4014.
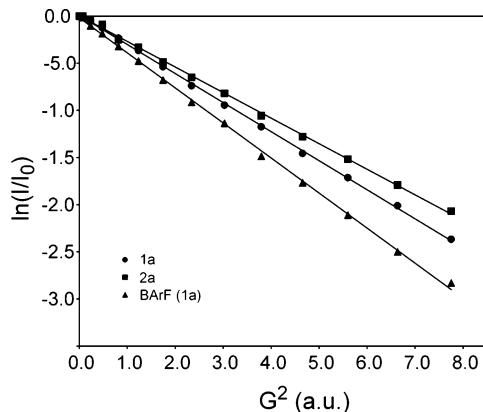
Figure 6. Plot of the observed intensity changes (I/I_0) vs arbitrary units proportional to the square of the gradient amplitude for PGSE measurements on **1a** and **2a** (CD_2Cl_2 solutions, 60 mM solutions). The lines represent linear least-squares fits to the experimental data.

expected to have a significantly smaller hydrodynamic radii for the cation (ca. 7 Å or less[63]).

Crucially, with regard to the solution characterization of **1a** and **2a**, that the clusters remain intact in solution *and* have 12 hydride ligands is unequivocally shown by electrospray ionization mass spectrometry (ESI-MS[65]), which shows only the intact clusters and no other charged species.[66] ESI-MS on CH_2Cl_2 solutions of **1a** and **2a** under very soft conditions (cone voltage of 10 V, source and desolvation gas temperatures both 30 °C) are in full agreement with the formulation $[Rh_6(PR_6)_6H_{12}]^{2+}$, with a single molecular species observed at m/z 795.1 (calcd 795.2) for **1a** and 1155.5 (calcd 1155.7) for **2a**, which have experimentally determined isotope patterns that are an excellent match with theory (Figure 7).

Reversible Dihydrogen Uptake by the Clusters $[Rh_6H_{12}$-$(PR_3)_6]^{2+}$. The reversible uptake of hydrogen by molecular or extended materials (such as nanoclusters) is an area that is attracting significant current interest. Much of this interest has centered on the role that such species play in hydrogenation reactions (especially arene hydrogenation), in particular the nature of the actual species in catalysis (nanocluster versus molecular cluster)[1,9,10,32] and potential hydrogen storage applications.[33–35] Given the high hydride content of the clusters **1a** and **2a**, we reasoned that they may act as well-defined molecular *models* for the attachment of hydrogen on a metal

(65) Henderson, W.; McIndoe, J. S. *Mass Spectrometry of Inorganic and Organometallic Compounds*; John Wiley and Sons: Chichester, 2005.
(66) Butcher, C. P. G.; Dyson, P. J.; Johnson, B. F. G.; Khimyak, T.; McIndoe, J. S. *Chem. Eur. J.* **2003**, *9*, 944–950.
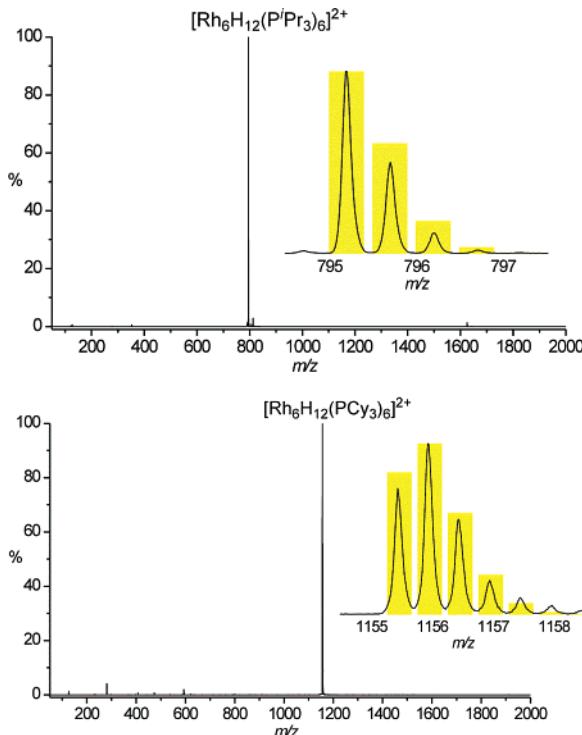
Figure 7. ESI-MS of **1a** (top) and **2a** (bottom) in CH₂Cl₂ solution. The inset shows the theoretically determined isotope patterns overlaid with experiment. Theoretical isotope patterns were calculated using Matthew Monroe's Molecular Weight Calculator (http://jjorg.chem.unc.edu/personal/monroe/mwtwin.html).

surface and/or hydrogen storage devices, and consequentally we investigated their reactivity with regard to dihydrogen uptake/loss.

Even though **1a** and **2a** have an exceptionally large number of hydride ligands, placing either cluster under a dynamic vacuum (10^{-3} Torr, 5 days, room temperature) did not result in loss of H₂, as measured by NMR spectroscopy and ESI-MS. In fact, the 12 hydride ligands are so firmly placed on the clusters that **1a** and **2a** can be routinely recrystallized from solutions containing an excess (>100-fold) of 1-hexene, and addition of an excess (>100-fold) of the excellent hydrogen acceptor *tert*-butylethylene (tbe) does not remove any of the 12 hydride ligands. This was at first surprising, but in light of the electronic structure of the clusters (vide infra) that affords a very stable 76 cve count, perhaps it should not be. Although H₂ is not lost either under vacuum or by addition of a hydrogen acceptor, *addition* of H₂ is facile and results in the immediate uptake of two molecules of H₂ to afford the octahedral clusters [Rh₆(PR₃)₆H₁₆][BArF₄]₂ (Scheme 4, R = ᶦPr (**1b**), Cy (**2b**)). This
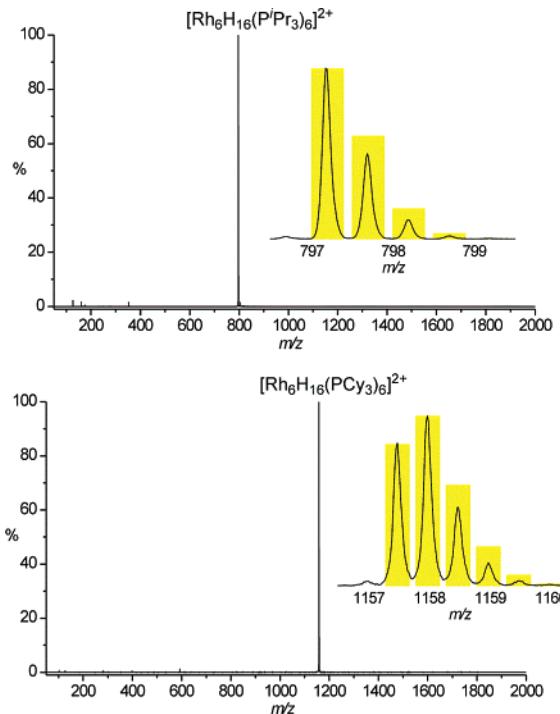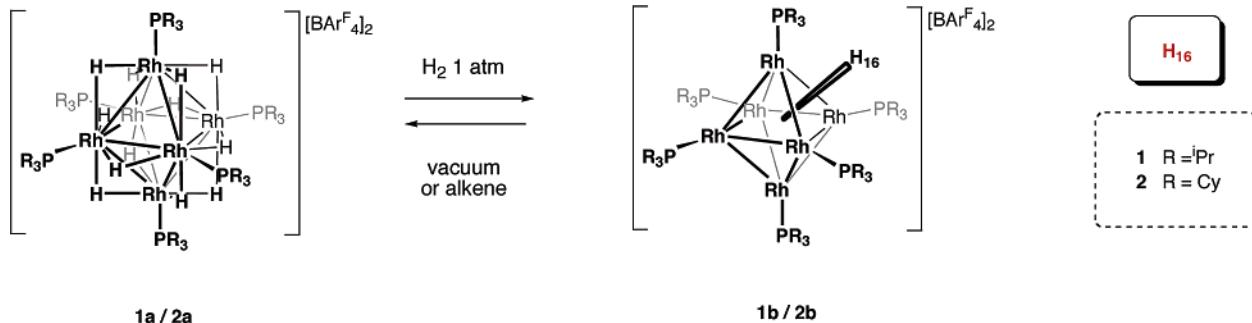

Figure 8. ESI-MS of **1a** and **2a** after addition of H₂ to afford **1b** (top) and **2b** (bottom).

hydrogen uptake occurs under mild conditions of temperature and pressure, happening at room temperature in CD₂Cl₂ solution under 1 atm of H₂ over ~10 min, and effectively instantaneously at room temperature under 4 atm of H₂. The uptake of hydrogen also occurs in the solid state by placing crystalline material under 4 atm of H₂. In this instance this solid-state reaction is, not unexpectedly, slower (16 h) and is also dependent on the size of the crystals. Pressurizing **1a** to 100 bar of H₂ in CD₂Cl₂ solution afforded only **1b**, showing that hydrogen uptake stops at two molecules of H₂. The ESI-MS spectra of **1b** and **2b** (CH₂-Cl₂ solutions under the mild conditions used previously) unambiguously show the uptake of two molecules of H₂ (an increase of m/z 2 = 4 Da for a 2+ cation to m/z 797.2 and 1157.5, respectively), displaying "flagpole spectra" with excellent isotope distribution match to the calculated patterns (Figure 8). Under the conditions used, the potential intermediate 14-hydride species was not observed.

The room-temperature ¹H NMR spectra (CD₂Cl₂ solutions) of **1b** and **2b** show resonances due to [BArF₄]⁻ anions and the alkyl phosphines in the appropriate ratio. In the high-field region, two hydride signals are observed in the ratio 15:1 with respect to both the anion and phosphine resonances. One of these is
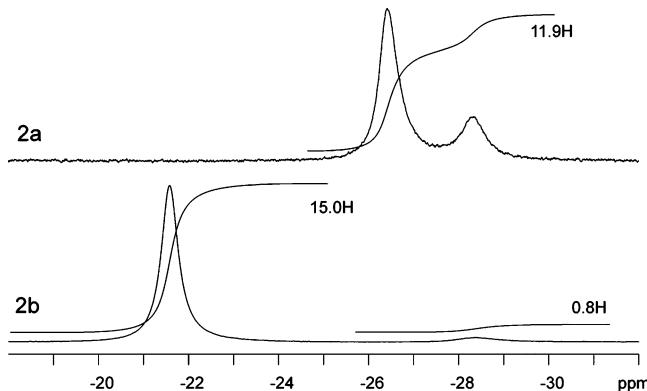
Scheme 4. Reversible Dihydrogen Uptake

1a / 2a   **1b / 2b**

Figure 9. High-field region of the room-temperature ^1H NMR spectra of **2a**/**2b**. Integrals are quoted relative to the alkyl phosphine protons.

relatively sharp, while the other is much broader, e.g., for **1b** δ −21.46 ppm (15 H, fwhm 40 Hz) and δ −29.81 ppm (1 H, fwhm 200 Hz). This pattern of integrals is consistent over a number of independently synthesized, crystalline samples. Figure 9 shows the high-field region for the pair **2a**/**2b**.

This 15:1 ratio suggests a structure in which 15 hydrides are mutually exchanging on the NMR time scale and one is not. Mutual exchange of the 15 hydrides is necessary, as it is not possible to arrange 15 hydrides around an octahedron symmetrically. To our minds, the only plausible structure that accounts for this observation is one that invokes an interstitial hydride with 15 hydride ligands decorating the outside of the Rh_6 octahedron. Interstitial hydrides are well-known in transition metal clusters and have been characterized by NMR spectroscopy and, in some cases, neutron diffraction techniques.[45,46,67] The chemical shift of interstitial hydrides can vary over a considerable range, for example δ +16.4 ppm for [HRu$_6$-(CO)$_{18}$]$^-$ [68] to δ −26.9 ppm for [HNi$_{12}$(CO)$_{21}$]$^-$,[69] and it has been suggested that hydrides that are located in the center of a regular octahedron show the lowest-field chemical shifts, while those more asymmetrically orientated have high-field chemical shifts.[70] For **2b**, an X-ray study (vide infra) shows a rather distorted octahedron, and thus a chemical shift observed for the unique hydride around δ −29 ppm is not unreasonable. DFT studies also indicate that a structure with 15 hydride ligands on the surface and one interstitial is significantly more stable than one with 16 hydrides on the surface, and these studies also show that this central hydride sits rather asymmetrically inside the Rh_6 core. Of course, in the absence of a neutron diffraction study, the assignment of an interstitial hydride must remain plausible but tentative, especially as examples exist of instances where interstitial hydrides have been originally proposed but later proven to be, in fact, located on the cluster surface.[71] The room-temperature $^{31}P\{^1H\}$ NMR spectra for both **1b** and **2b** show broad environments, which for **1b** resolves into a doublet J(RhP) = 140 Hz. Within error, the hydrodynamic radii of **1b** and **2b** as calculated using PGSE in CD$_2$Cl$_2$ solutions are the same as for **1a**/**2a** [9.5(3) and 10.3(5) Å,[3] respectively].

On cooling of **1b** and **2b** to 200 K (CD$_2$Cl$_2$), their hydride resonances become broader and resolve into many separate signals with an overall integral lower than 16 H, both being nearer 12 H, showing that the hydrides are mobile over the surface of the cluster at room temperature. The broad linewidths of some of these signals indicate that any fluxional processes occurring are not completely frozen out at 200 K, as does the lower-than expected integral value. T_1 measurements at 200 K indicate that all the *observed* signals are best assigned to hydride ligands (T_1 > 230 ms), although the presence of two unresolved dihydrogen ligands in the baseline cannot be discounted. Higher temperatures (up to 350 K, 1,2-difluorobenzene solvent) result in the apparent coalescence of the two peaks, possibly suggesting exchange, although as the integral 1 H peak is very broad, it could simply be unresolved in the baseline. At this temperature, partial decomposition of the cluster to unidentified material is also observed. Under a H$_2$ atmosphere (1 atm) at 298 K, dissolved H$_2$ is observed as a sharp resonance at δ 4.6 ppm, demonstrating that exchange between free and bound H$_2$ is slow on the NMR time scale. Slow exchange with free H$_2$ does occur, however, as placing **1b** or **2b** under a D$_2$ atmosphere (∼4 atm) results in complete H/D exchange for the hydride ligands in 72 h and the appearance of HD as a characteristic 1:1:1 triplet at δ 4.55 ppm [J(DH) = 43 Hz], along with H$_2$. The observation of HD and free H$_2$ suggests coordinated dihydrogen on the cluster surface, resulting from H/D exchange via a dihydrogen intermediate.[51,61] To our knowledge, the only cluster identified as containing a dihydrogen ligand (as identified by T_1 measurements and DFT calculations) is [Ru$_4$H$_6$(C$_6$H$_6$)$_4$]$^{2+}$,[51] although bimetallic complexes with dihydrogen ligands are known,[61,72] and dihydrogen complexes have been suggested to be possible intermediates in clusters that catalyze H$_2$−D$_2$ equilibration to form HD.[73,74] Interestingly, after 3 days under D$_2$ at 313 K, for **1b** some deuterium is also incorporated into the isopropyl groups on the phosphines (as shown by ^2H NMR and ESI-MS), suggesting that these ligands do not play a completely innocent role in the clusters. We have not yet pursued the mechanism of H/D exchange, but it is likely that it involves reversible oxidative addition of an alkyl C−H bond to the cluster core.

Despite repeated attempts, the crystalline material of **1b** afforded X-ray diffraction patterns that indicated high levels of disorder. Crystals suitable for X-ray diffraction for **2b** where grown using the alternative anion [1-H-CB$_{11}$Me$_{11}$]$^-$ [40] from CH$_2$-Cl$_2$/pentane solution under 1 atm of H$_2$. Crystals of the [BAr$^F_4$]$^-$ salt of **2b** were of marginal quality, and the structure obtained is not reported here. Nevertheless, the resulting cluster core structural metrics are essentially the same as for that with the [1-H-CB$_{11}$Me$_{11}$]$^-$ anion, demonstrating that the anions do not

(67) Bau, R.; Drabnis, M. H. *Inorg. Chim. Acta* **1997**, *259*, 27−50. Bau, R.; Drabnis, M. H.; Garlaschelli, L.; Klooster, W. T.; Xie, Z. W.; Koetzle, T. F.; Martinengo, S. *Science* **1997**, *275*, 1099−1102. Adams, R. D.; Babin, J. E.; Tanner, J. T. *Organometallics* **1988**, *7*, 2027−2033. Hart, D. W.; Teller, R. G.; Wei, C. Y.; Bau, R.; Longoni, G.; Campanella, S.; Chini, P.; Koetzle, T. F. *Angew. Chem., Int. Ed. Engl.* **1979**, *18*, 80−81. Eady, C. R.; Johnson, B. F. G.; Lewis, J.; Malatesta, M. C.; Machin, P.; McPartlin, M. *J. Chem. Soc., Chem. Commun.* **1976**, 945−946. Broach, R. W.; Dahl, L. F.; Longoni, G.; Chini, P.; Schulz, A. J.; Williams, J. M. *Adv. Chem. Ser.* **1978**, *167*, 93.

(68) Eady, C. R.; Jackson, P. F.; Johnson, B. F. G.; Lewis, J.; Malatesta, M. C.; McPartlin, M.; Nelson, W. J. H. *J. Chem. Soc., Dalton Trans.* **1980**, 383−392.

(69) Eguchi, T.; Heaton, B. T.; Harding, R.; Miyagi, K.; Longoni, G.; Nahring, J.; Nakamura, N.; Nakayama, H.; Pakkanen, T. A.; Pursiainen, J.; Smith, A. K. *J. Chem. Soc., Dalton Trans.* **1996**, 625−630.

(70) Eguchi, T.; Heaton, B. T. *J. Chem. Soc., Dalton Trans.* **1999**, 3523−3530.

(71) Bashall, A.; Gade, L. H.; Lewis, J.; Johnson, B. F. G.; McIntyre, G. J.; McPartlin, M. *Angew. Chem., Int. Ed. Engl.* **1991**, *30*, 1164−1167.

(72) Sola, E.; Bakhmutov, V. I.; Torres, F.; Elduque, A.; Lopez, J. A.; Lahoz, F. J.; Werner, H.; Oro, L. A. *Organometallics* **1998**, *17*, 683−696.

(73) Aubart, M. A.; Chandler, B. D.; Gould, R. A. T.; Krogstad, D. A.; Schoondergang, M. F. J.; Pignolet, L. H. *Inorg. Chem.* **1994**, *33*, 3724−3734.

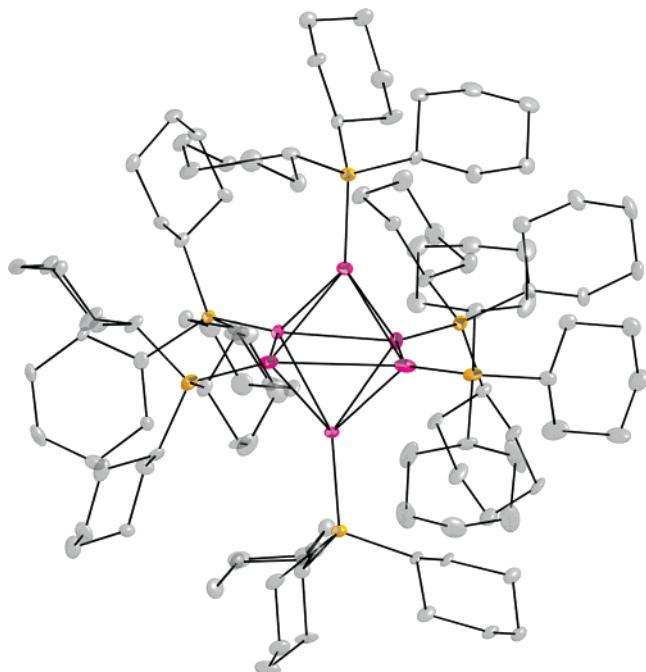(74) Aime, S.; Dastru, W.; Gobetto, R.; Krause, J.; Matas, L.; Viale, A. *Organometallics* **1996**, *15*, 4967−4970.

Figure 10. Solid-state structure of the dication of **2b**[HCB$_{11}$Me$_{11}$]$_2$. Thermal ellipsoids are shown at the 50% probability level. The counterions are not shown. The hydride ligands around the cluster core were not located reliably. All other hydrogen atoms have been omitted for clarity. See Supporting Information for labeling scheme.

have a pronounced effect on the cluster geometry. Figure 10 shows the solid-state structure of **2b**[1-H-CB$_{11}$Me$_{11}$]$_2$. Selected structural comparisons are given in Table 2.

The cluster core in **2b** describes an approximate octahedron, but compared to the H$_{12}$-hydride counterparts **1a** and **2a** it is significantly distorted. Notably, the Rh—Rh distances span a wider range, δ(Rh—Rh) being an order of magnitude larger for the H$_{16}$ species than the H$_{12}$ clusters. The cross-cluster Rh···Rh and P···P distances are also larger and span a similarly wide range. The cross-cluster Rh···Rh—P angles also span a much wider range for **2b** than for **2a**, e.g., 178.3(1)−177.7(1)° for **2a** and 177.1(1)−166.8(1)° for **2b**. The hydride ligands around the {Rh$_6$} core were not located with any certainty. As discussed, the location of hydrogen atoms near metal centers is always potentially problematic, and coupled with the fact that the hydrides in **2b** will be distributed asymmetrically in the solid state, potentially leading to partial occupancy of sites, this means that the definitive location of the hydrides using X-ray crystallography would always be difficult. Nevertheless, the combination of NMR and ESI-MS data unambiguously points to clusters with 16 hydride ligands. Moreover, the structural comparisons between the 12-hydride clusters, **1a/2a**, and the 16-hydride cluster, **2b**, indicate the accommodation of four extra hydride ligands in the latter by significantly larger Rh—Rh distances and deviations, larger cross-cluster Rh···Rh distances, and greater deviations from linearity for Rh···Rh—P angles. These structural variations are underscored by DFT calculations on both 12- and 16-hydride structures (vide infra) that, for comparison, are shown in Table 2. Even though the phosphine PH$_3$ was used in the DFT model instead of the bulky P^{i}Pr$_3$ or PCy$_3$ ligands, all the changes observed experimentally on addition of dihydrogen are reproduced satisfactorily in the calculated structures.
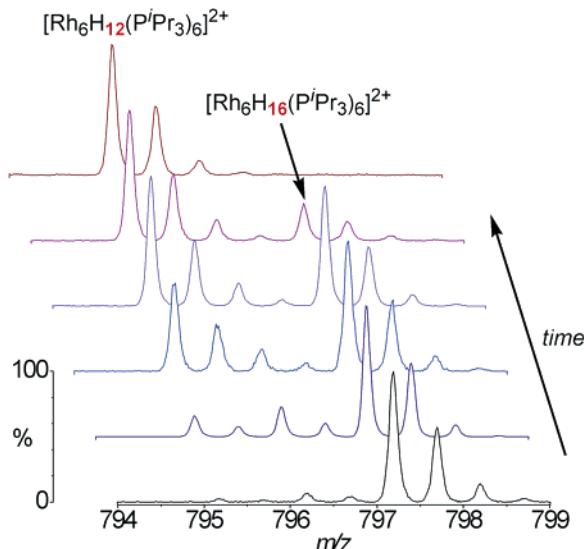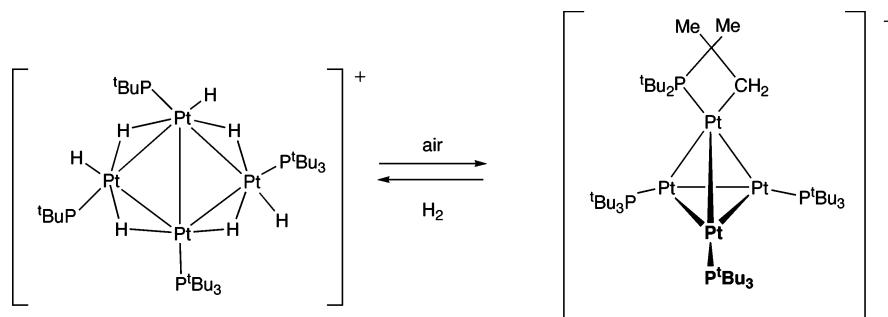

Figure 11. Stacked plot of ESI-MS of **1b** on addition of the hydrogen acceptor *tert*-butylethene ($\sim$100-fold excess) in CH$_2$Cl$_2$ solution. The bottom spectrum was obtained 5 min after addition of tbe and the top after 24 h.

The 16-hydride complex **2a** slowly loses H$_2$ in the solid state under an argon atmosphere to give **1a**, giving a ratio of 1:0.7 for **2a**:**1a** by ^{1}H NMR spectroscopy after 1 week. By contrast, after 1 week **2b** is unchanged as shown by NMR and ESI-MS. Under vacuum (5 × 10^{-3} Torr), H$_2$ loss is faster. For the ^{i}Pr$_3$P cluster, **1b**, complete H$_2$ loss is considerably more rapid (12 h) than for the PCy$_3$ congener **2b** ($\sim$1 week). This increased resistance to H$_2$ loss for **2b** reflects the increased kinetic stabilization toward H$_2$ loss provided by the bulky cyclohexyl ligands, as electronically both **1b** and **2b** would be expected to be very similar. This process is completely reversible for both clusters, and repressurizing with H$_2$ regenerates quantitatively (NMR, ESI-MS) the H$_{16}$ species. Loss of two hydrogen molecules is also effected by addition of hydrogen acceptors such as *tert*-butylethene or 1-hexene, as monitored by NMR and ESI-MS (Figure 11). The loss of dihydrogen from **1b** or **2b** is not at odds with their putative interstitial hydride structure, as interstitial hydrides in octahedral complexes have been noted to be mobile between the center of the octahedron and the cluster surface. For example, protonation of [Ru$_6$(μ_6-H)(CO)$_{18}$]$^-$ affords H$_2$Ru$_6$(CO)$_{18}$, which has two bridging hydrides,[68] while the interstitial hydride in [Co$_6$(μ_6-H)(CO)$_{15}$]$^-$ undergoes rapid migration from the inside to the outside of the cluster.[46,69,70]

Although complexes with hydride ligands are common in cluster chemistry, those that can *reversibly* take up and release one molecule of H$_2$ are few.[73,75,76] Of these species that reversibly take up H$_2$, only one approaches the high hydride count of **1b/2b**, [Pt$_4$H$_7$(P^{t}Bu$_3$)$_4$][BF$_4$].[48] This cluster reversibly loses four molecules of H$_2$ on exposure to air, to afford a cluster with no hydrides (Scheme 5), or on exposure to ethene, to give a cluster with one hydride ligand. Pt$_3$Re$_2$(CO)$_6$(P^{t}Bu$_3$)$_3$ has been reported to take up a relatively large amount of H$_2$ (3 equiv), but the process is not reported to be reversible for this cluster.[18,76]

(75) Safarowic, F. J.; Bierdeman, D. J.; Keister, J. B. *J. Am. Chem. Soc.* **1996**, *118*, 11805−11812. Farrugia, L. J.; Green, M.; Hankey, D. R.; Orpen, A. G.; Stone, F. G. A. *J. Chem. Soc., Chem. Commun.* **1983**, 310−312. Arif, A. M.; Bright, T. A.; Jones, R. A.; Nunn, C. M. *J. Am. Chem. Soc.* **1988**, *110*, 6894−6895.
(76) Adams, R. D.; Captain, B.; Smith, M. D. *Angew. Chem., Int. Ed.* **2006**, *45*, 1109−1112.
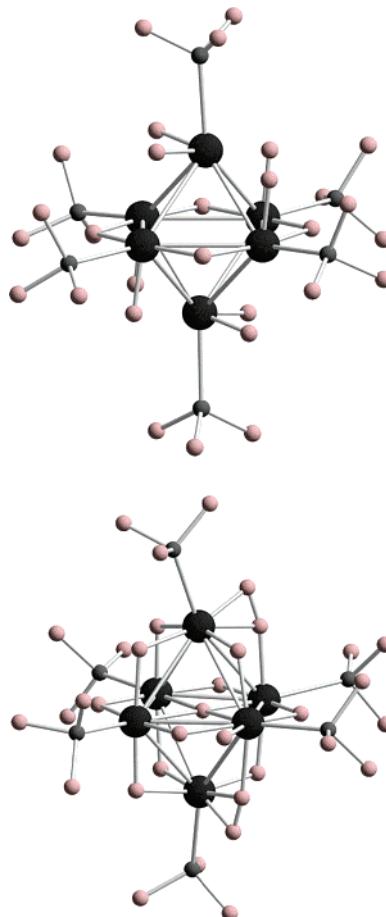
Scheme 5. Reversible H$_2$ Uptake in [Pt$_4$H$_7$(P^{t}Bu$_3$)$_4$][BF$_4$]

The cluster species [Rh$_6$(PR$_3$)$_6$H$_{16}$][BAr$^F_4$]$_2$ are thus unique in that H$_2$ uptake and loss is facile and the "low" hydride species that result still have an exceptionally high number of hydrides. To our knowledge, the complexes **1b** and **2b** are without precedent in cluster chemistry, combining (i) the greatest number of hydride ligands so far reported on a discrete metal cluster, (ii) a hydride:metal ratio of greater than 2:1 (Pd$_{28}$(PtPMe$_3$)-(PtPPh$_3$)$_{12}$(CO)$_{27}$H$_{12}$[50] has 12-hydride ligands but has 41 metals in its core, while [Ir$_3$(PHOX)$_3$H$_7$][PF$_6$]$_2$[55] has a high hydride: metal ratio of 7:3 but only seven hydride ligands[54,55]), and (iii) reversible hydrogen loss/uptake of two molecules of H$_2$.

DFT Calculations on the Model Cluster Pairs [Rh$_6$-(PH$_3$)$_6$H$_{12}$]$^{2+}$ and [Rh$_6$(PH$_3$)$_6$H$_{16}$]$^{2+}$. DFT calculations on the cluster pair [Rh$_6$(PH$_3$)$_6$H$_{12}$]$^{2+}$ and [Rh$_6$(PH$_3$)$_6$H$_{16}$]$^{2+}$ have been carried out at the ADF/TZVP level, with the alkyl phosphine groups substituted by PH$_3$ for computational expediency. Full details of these calculations, the molecular orbital description of the bonding, and the hydrogen uptake will appear in a dedicated full paper. Here we briefly outline the main conclusions and highlight how these calculations mirror the experimentally determined results and support the assignment of the hydride count for the cluster pairs **1a/1b** and **2a/2b**. We also comment briefly on the molecular orbital structure of the 12-hydride species.

Figure 12 shows the calculated structures for [Rh$_6$(PH$_3$)$_6$H$_{12}$]$^{2+}$ and [Rh$_6$(PH$_3$)$_6$H$_{16}$]$^{2+}$, and Table 2 presents selected structural metrics for the pair, alongside the experimentally determined structures from single-crystal X-ray diffraction. Although the substitution of bulky P^{i}Pr$_3$ or PCy$_3$ for the model phosphine PH$_3$ might be expected to have a significant effect on the cluster geometry, that there is a surprisingly good correlation between theory and experiment shows that, although bulky, the phosphine ligands exert less influence on the cluster core than might be expected. Dealing with the {Rh$_6$P$_6$} cluster cores first, all the observed structural trends on going from H$_{12}$ to H$_{16}$ are mirrored in the DFT-calculated structures (Table 2). Specifically, on addition of two molecules of H$_2$, the octahedron becomes significantly less regular, Rh–Rh distances get significantly larger, as do their range of distances, the cross-cluster Rh···Rh distances become larger, and the Rh···Rh–P angles deviate more from linear in the 16-hydride cluster. The hydride ligands in calculated [Rh$_6$(PH$_3$)$_6$H$_{12}$]$^{2+}$ describe two distinct bonding motifs: four symmetrically bridging around a central octahedral plane, and the remaining eight that can be considered semi-bridging/terminal. The underlying electronic reasons for this will be discussed in a more detailed contribution, but pleasingly, this arrangement is partially reflected in the crystal structure of **1a**, which shows six hydrides to be semi-bridging within the

precision afforded by an X-ray diffraction experiment. Addition of two molecules of H$_2$ to give [Rh$_6$(PH$_3$)$_6$H$_{16}$]$^{2+}$ has been modeled in two ways: by 16 hydrides on the surface of the polyhedron, and by 15 on the surface and 1 central (interstitial). The interstitial model comes out as being significantly more stable by 145 kJ mol^{-1}, in line with the experimental NMR data that show a 15:1 ratio of hydride ligands. Of the 15 hydrides on the outside of the octahedron, four of them (two pairs) have short H–H distances, indicative of dihydrogen ligands, d(H–H) = 1.061 and 0.965 Å. Similar structures, implicating a mixture of dihydrogen and hydride ligands, have been calculated for Pd$_5$H$_6$ clusters.[77] The presence of dihydrogen ligands is consistent with the experimental observations that the cluster undergoes H/D exchange with D$_{2(g)}$ to produce HD$_{(g)}$ and that the low-temperature, high-field ^{1}H NMR spectra of both **1b** and **2b** show a total integral of 12 H, the four missing protons

Figure 12. DFT-calculated structures of [Rh$_6$(PH$_3$)$_6$H$_{12}$]$^{2+}$ (top) and [Rh$_6$-(PH$_3$)$_6$H$_{16}$]$^{2+}$ (bottom).

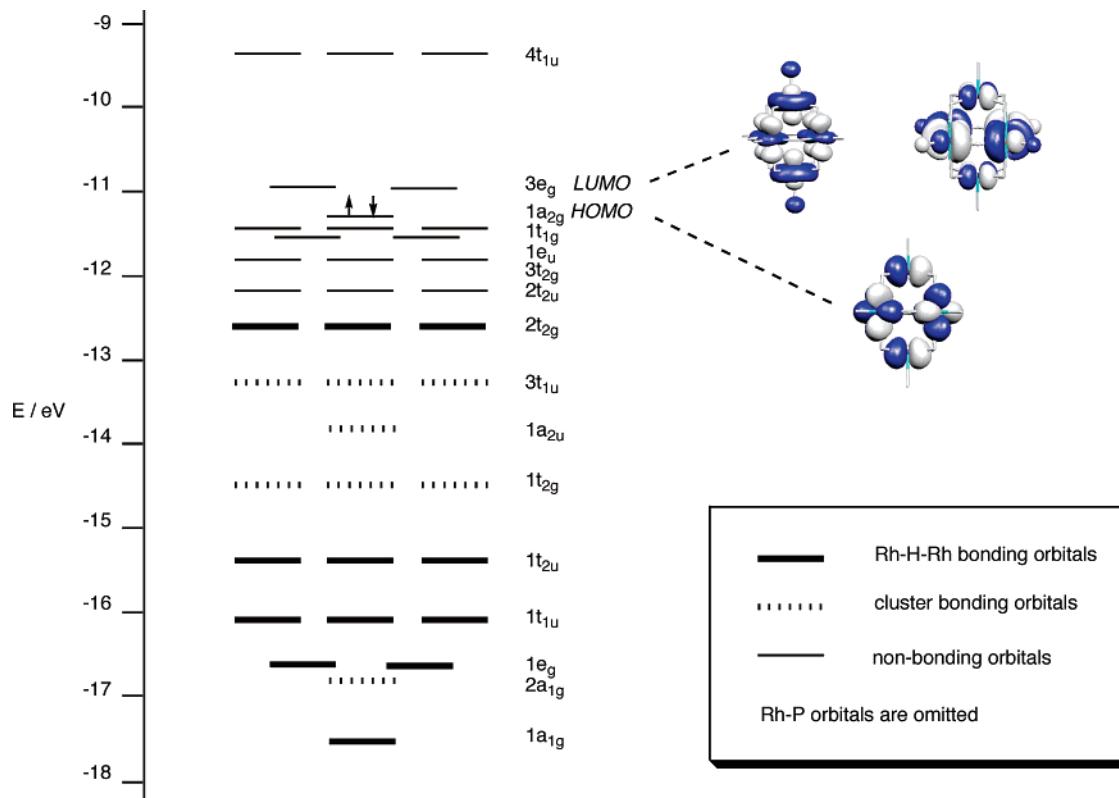**Figure 13.** Partial molecular orbital diagram for $[Rh_6(PH_3)_6H_{12}]^{2+}$ under the constraint of O_h symmetry, showing the orbitals involved with cluster bonding. Diagrammatic representations of the HOMO and LUMO orbitals are also shown.

presumably broad and not observed. Also consistent with the ^1H NMR data is that the interstitial hydride is not located in the geometric center of the cluster, with the internal Rh−H distances varying between 2.082 and 1.875 Å in the model. The dissociation energy of the two H_2 molecules from the H_{16} cluster, i.e., the SCF energy difference between $[Rh_6H_{12}(PH_3)_6]^{2+}$ + $2H_2$ and $[Rh_6H_{16}(PH_3)_6]^{2+}$, is calculated as 151 kJ mol^{-1} in favor of the $[Rh_6H_{16}(PH_3)_6]^{2+}$ cluster.

In terms of simple electron book-keeping, the 12 hydride clusters **1a** and **2a** have 76 cve, this being 10 cve less than that found for late transition metal octahedral clusters (86 cve) such as $Rh_6(CO)_{16}$. However, the electron count is exactly like that of the early transition metal clusters such as $[Nb_6Cl_{18}]^{4-}$ and is similar to that of the structurally closely related zirconium-phosphine clusters $Zr_6Cl_{12}(PMe_2Ph)_6$ (72 cve)[56] and $Zr_6Cl_{14}H_4$-$(PMe_3)_4$ (74 cve).[4] Dicationic hexanuclear clusters $[Au(PR_3)]_6^{2+}$ of 76 cve are also known, and these can adopt either octahedral[78] or edge-shared bitetrahedral structures.[79] The structural similarity between the early transition metal clusters with edge-bridged halides (Scheme 1) and **1a/2a**, with 12 edge-bridged hydrides, is remarkable and underscores that both sets of clusters are built from {ML$_5$} fragments, e.g., {ClNbCl$_4$} and {(PR$_3$)RhH$_4$}. The molecular orbital description of clusters such as $[Nb_6Cl_{18}]^{4-}$ is well understood,[16] and cluster bonding arises from 8 cluster bonding orbitals. By comparison, calculations on $[Rh_6(PH_3)_6$-$H_{12}]^{2+}$, with the $Rh_6P_6H_{12}$ core constrained to octahedral symmetry for simplicity, revealed 20 bonding and 12 nonbond-

ing cluster orbitals (Figure 13). Of these, 12 may be regarded as built from the 12 three-center, two-electron Rh−H−Rh bonds ($1a_{1g}$, $1e_g$, $1t_{1u}$, $1t_{2u}$, and $2t_{2g}$ in symmetry); these are equivalent to the Nb−Cl−Nb symmetric bonding orbitals. The other 20 are principally metal-localized and correspond to the 8 Nb−Nb bonding orbitals of the niobium cluster ($2a_{1g}$, $1t_{2g}$, $3t_{1u}$, and $1a_{2u}$ in symmetry) and 12 metal-localized orbitals ($2t_{2u}$, $3t_{2g}$, $1e_u$ $1t_{1g}$, and $1a_{2g}$ in symmetry), which are numerically equal (though not symmetrically equivalent) to the 12 antisymmetric Nb−Cl−Nb bridging bonds; the π-donor interaction of the 12 Cl's with the Nb_6 core is replaced in the Rh_6H_{12} cluster by metal-localized electrons. The remaining 6 orbitals that complete a total orbital count of 38 (and consequently an electron count of 76) are associated with Rh−P bonding ($2t_{1u}$, $2e_g$, and $3a_{1g}$). Replacing the chlorides in $[Nb_6Cl_{18}]^{4-}$ with hydrides and phosphines reduces the overall electron count by 24, but moving from a group 5 metal to a group 9 metal results in a net gain of 24 electrons to the cluster. Thus, the low ligand electron count of $[Rh_6(PH_3)_6H_{12}]^{2+}$ is exactly balanced by the move from Nb to Rh and the subsequent use of 12 additional metal-localized orbitals (and 24 electrons). Although with regard to octahedral late transition metal clusters composed of {ML$_3$} fragments such as $Rh_6(CO)_{16}$ **1a** and **2a** count less by 10 electrons, they are in fact electron-precise for a cluster constructed from {ML$_5$} fragments such as $[Nb_6Cl_{18}]^{4-}$.

The principal difference in the orbital structure when the symmetry is lowered from octahedral to that of the optimized calculated structure is that two of the three Rh−H−Rh $2t_{2g}$ orbitals are considerably stabilized by the shift of eight hydrogens from central bridging to semi-bridging positions as a consequence of improved overlap between the H 1s orbitals

(77) Moc, J.; Musaev, D. G.; Morokuma, K. *J. Phys. Chem. A* **2003**, *107*, 4929−4939.
(78) Bellon, P.; Manasser, M.; Sansoni, M. *J. Chem. Soc., Dalton Trans.* **1973**, 2423−2427.
(79) Briant, C. E.; Hall, K. P.; Mingos, D. M. P.; Wheeler, A. C. *J. Chem. Soc., Dalton Trans.* **1986**, 687−692.
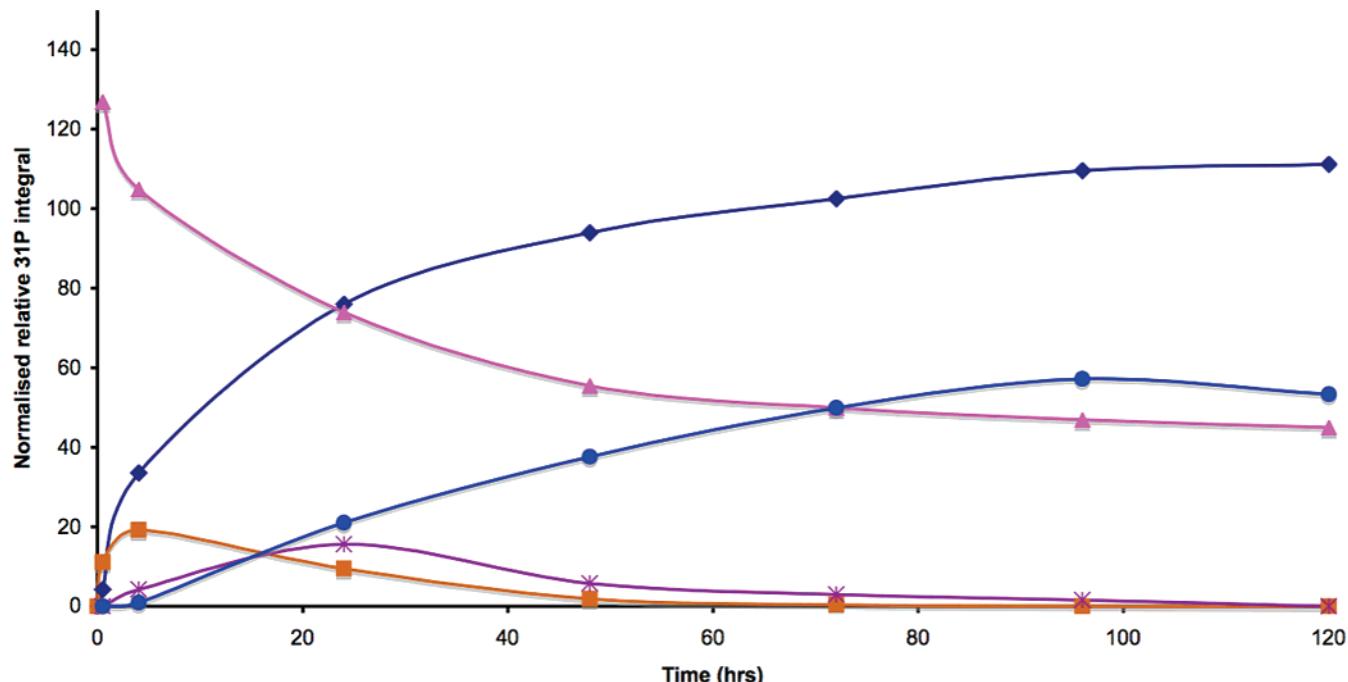
Figure 14. Time versus relative ^{31}P integral plot for the synthesis of cluster **1b**. ▲, "Rh(P^{i}Pr$_3$)$_2$" species at δ(^{31}P) 64−58 ppm, see text; ♦, [HP^{i}Pr$_3$][BAr$^F_4$]; ●, **1b**[BAr$^F_4$]$_2$; ∗, [RhH$_2$(P^{i}Pr$_3$)(η^6-C$_6$H$_6$)][BAr$^F_4$]; ■, [RhH$_2$(P^{i}Pr$_3$)(η^6-C$_6$H$_5$F)][BAr$^F_4$].

and the Rh 4d orbitals. Mixing between a 3e$_g$ orbital and the 1a$_{2g}$ orbital localizes a pair of electrons in the same plane as the symmetrically bridging hydrogens.

The HOMO−LUMO gap in [Rh$_6$(PH$_3$)$_6$H$_{12}$]$^{2+}$ as calculated under O_h symmetry is relatively small, ∼0.3 eV, and the LUMO is of e$_g$ degeneracy and effectively nonbonding. These two observations suggests that addition of four electrons should be facile. These four electrons can come from two molecules of H$_2$, and addition results in the 16-hydride, 80 cve species [Rh$_6$-(PH$_3$)$_6$H$_{16}$]$^{2+}$ having a much larger HOMO−LUMO gap of 1.3 eV, which disfavors the addition of further hydrogen, as is observed experimentally. A similar analysis of frontier molecular orbitals has previously been used to account for the facile uptake of three molecules of H$_2$ by the electronically unsaturated cluster Pt$_3$Re$_2$(CO)$_6$(P^{t}Bu$_3$)$_3$, to give Pt$_3$Re$_2$(CO)$_6$(P^{t}Bu$_3$)$_3$H$_6$ with no major structural change.[18]

The full molecular orbital structure description, discussion of the facile uptake of H$_2$, and electron counting for the clusters will be dealt with in detail in a future full paper. Importantly for this paper, which deals with the synthesis and structures of these new clusters, the structural descriptors of the H$_{12}$ and H$_{16}$ complexes are reproduced very well in the DFT calculations, which give confidence to the assignment of the solid-state structures of the cluster pair **1a**/**1b** as well as **2b**.

Mechanism of Cluster Formation. As discussed in the Introduction, clusters that form under kinetic conditions are relatively unusual, and the attractive time scales (5 days) and moderate temperatures involved (313−323 K) in the formation of **1a** and **2a** afford a rare opportunity to probe a cluster self-assembly process using NMR spectroscopy. Addition of H$_2$ (∼4 atm) to a fluorobenzene solution of [Rh-(P^{i}Pr$_3$)$_2$(nbd)][BAr$^F_4$] in a sealed J. Youngs tube initially results in the formation of the almost colorless dihydrogen/dihydride complexes [Rh-(P^{i}Pr$_3$)$_2$(H)$_2$(η^2-H$_2$)$_x$][BAr$^F_4$] (x = 1 or 2), as shown by a broad ^{31}P{^{1}H} NMR resonance at δ 63 ppm and a very broad signal

at δ −5.8 ppm in the ^{1}H NMR spectrum at high field.[39] Following the reaction by NMR spectroscopy during gentle heating at 313 K over 5 days revealed a number of intermediate species, along with the final product **1b** that forms from addition of H$_2$ to **1a**. Figure 14 shows a graph of integrated ^{31}P resonances against time for this experiment.

There are three new species observed after 2 h of reaction in the ^{31}P{^{1}H} NMR spectrum. The first is [HP^{i}Pr$_3$][BAr$^F_4$],[80] identified by a distinctive resonance at δ 46 ppm which splits into a doublet, J(PH) = 336 Hz, in the ^{31}P NMR spectrum. Using D$_2$ in the reactions rather than H$_2$ afforded [DP^{i}Pr$_3$]-[BAr$^F_4$] and, ultimately **1b-d_{16}**. The second new species is a very small amount of cluster **1b**. Both of these species continue to increase in concentration throughout the experiment. The third new species is spectroscopically identified as the fluorobenzene complex [RhH$_2$(P^{i}Pr$_3$)(η^6-C$_6$H$_5$F)][BAr$^F_4$] (**3**). Complex **3** has been independently synthesized by addition of H$_2$ to [(binor-*S*)Rh(P^{i}Pr$_3$)][BAr$^F_4$] (a source of a reactive {Rh(PR$_3$)}$^+$ fragment)[81] in fluorobenzene solution (Scheme 6), and the NMR data match exactly those observed in the reaction mixture.

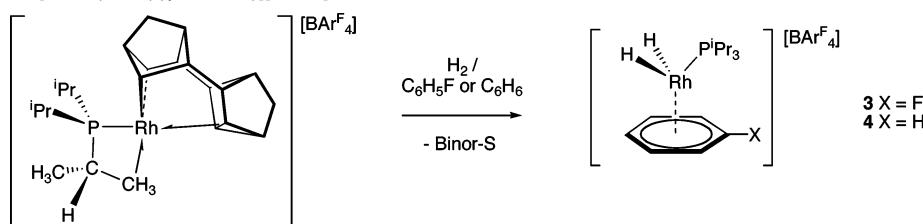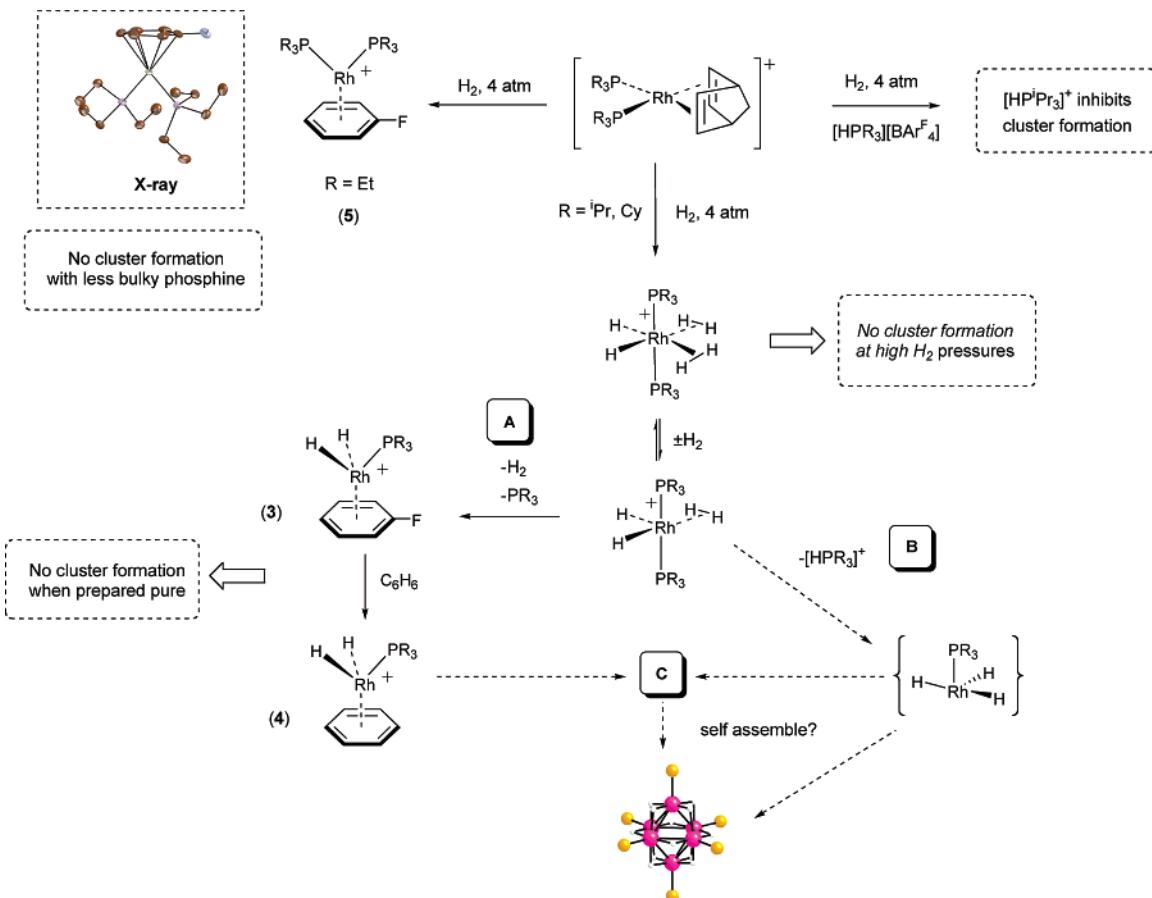After 3 h the concentration of complex **3** drops, to be replaced by a species identified as the benzene complex [RhH$_2$(P^{i}Pr$_3$)-(η^6-C$_6$H$_6$)][BAr$^F_4$] (**4**).[82] Concomitant with the appearance of **4**, free benzene also appears in the ^{1}H NMR spectrum (δ 7.21 ppm) as well as traces of fluorocyclohexane (C$_6$H$_{11}$F, identified by a characteristic d of t of t at δ 4.40 ppm[83]). The generation of benzene most likely comes from hydrido-defluorination of fluorobenzene by traces of colloidal Rh, while hydrogenation

(80) Torres, F.; Sola, E.; Martin, M.; Lopez, J. A.; Lahoz, F. J.; Oro, L. A. *J. Am. Chem. Soc.* **1999**, *121*, 10632−10633.
(81) Brayshaw, S. K.; Green, J. C.; Sceats, E.; Kociok-Kohn, G.; Weller, A. S. *Angew. Chem., Int. Ed.* **2006**, *45*, 452−456.
(82) Canepa, G.; Brandt, C. D.; Ilg, K.; Wolf, J.; Werner, H. *Chem. Eur. J.* **2003**, *9*, 2502−2515.
(83) Lambert, J. B.; Greifenstein, L. G. *J. Am. Chem. Soc.* **1974**, *96*, 5120−5124.

Scheme 6. Synthesis of [RhH$_2$(P^{i}Pr$_3$)(η^6-C$_6$H$_5$X)][BAr$^F_4$]

Scheme 7. Observed Species in the Cluster Buildup Reaction and Suggested Mechanistic Routes (Dashed Arrows)^a
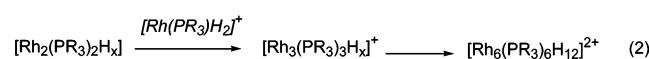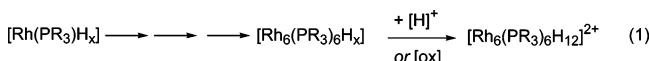

^{a} [BAr$^F_4$]$^-$ anions not shown.

of fluorobenzene to form fluorocyclohexane is also catalyzed by colloidal Rh.[84] The benzene thus produced readily displaces the weakly bound fluorobenzene in **3** to give **4**. After about 22 h, complex **4** starts to disappear, so by the end of the monitoring experiment the concentrations of **3** and **4** are both zero. During this time, the peak at δ 63 ppm in the ^{31}P{^{1}H} NMR spectrum gradually moves to being a doublet at δ 58.2 ppm [J(RhH) = 110 Hz] and reaches what appears to be an equilibrium concentration of approximately half the initial concentration of starting material. We assign this peak at δ 58.2 ppm to [Rh-(P^{i}Pr$_3$)$_2$(H)$_2$(η^2-H$_2$)][BAr$^F_4$], formed from loss of one H$_2$ from [Rh(P^{i}Pr$_3$)$_2$(H)$_2$(η^2-H$_2$)$_2$][BAr$^F_4$], as has been noted to happen when the H$_2$ pressure drops from ~4 atm to ~1−2 atm.[39] The final products of the reaction after 5 days are **1b**, [HP^{i}Pr$_3$]-[BAr$^F_4$], and [Rh(P^{i}Pr$_3$)$_2$(H)$_2$(η^2-H$_2$)][BAr$^F_4$]. Repeating the experiment under 100 bar H$_2$ did not afford the cluster, with

the only observed species being [Rh(P^{i}Pr$_3$)$_2$(H)$_2$(η^2-H$_2$)$_2$][BAr$^F_4$]. Removal of H$_2$ under vacuum after the initial hydrogenation of [Rh(nbd)(P^{i}Pr$_3$)$_2$][BAr$^F_4$] stopped the reaction and afforded the previously spectroscopically characterized complex [Rh(P^{i}Pr$_3$)$_2$-(H)$_2$(L)$_2$][BAr$^F_4$] (L = solvent or agostic interaction).[39] Use of less bulky phosphine ligands, such as PEt$_3$ (cone angle 132° [41]), starting from [Rh(nbd)(PEt$_3$)$_2$][BAr$^F_4$], cleanly affords the Rh-(I) species [Rh(η^6-C$_6$H$_5$F)(PEt$_3$)$_2$][BAr$^F_4$] (**5**), which has a coordinated fluorobenzene ligand and no hydride ligands (see Supporting Information for full characterization). On addition of H$_2$ no cluster is formed under 4 atm of H$_2$ on heating to 323 K, with **5** remaining unchanged. This suggests that phosphines with sufficient steric bulk to force the trans arrangement observed in [Rh(P^{i}Pr$_3$)$_2$(H)$_2$(η^2-H$_2$)$_2$][BAr$^F_4$] are required for cluster formation.

Scheme 7 outlines the species observed by NMR spectroscopy. That cluster formation does not occur under very high pressures of H$_2$, but also requires some H$_2$ to be available, shows that the bis-dihydrogen complex [Rh(P^{i}Pr$_3$)$_2$(H)$_2$(η^2-H$_2$)$_2$][BAr$^F_4$]

(84) Yang, H.; Gao, H.; Angelici, R. J. *Organometallics* **1999**, *18*, 2285−2287. Blum, J.; Rosenfeld, A.; Gelman, F.; Schumann, H.; Avnir, D. *J. Mol. Catal. A* **1999**, *146*, 117−122.

Scheme 8. Comparison of Possible Mechanisms Leading to Cluster Formation[a]

$$[Rh(PR_3)H_x] \longrightarrow \longrightarrow \longrightarrow [Rh_6(PR_3)_6H_x] \xrightarrow[\text{or [ox]}]{+ [H]^+} [Rh_6(PR_3)_6H_{12}]^{2+} \quad (1)$$

$$[Rh_2(PR_3)_2H_x] \xrightarrow{[Rh(PR_3)H_2]^+} [Rh_3(PR_3)_3H_x]^+ \longrightarrow [Rh_6(PR_3)_6H_{12}]^{2+} \quad (2)$$

[a] The number of hydrogen atoms (H_x) is arbitrary in each step.

is not an intermediate, but instead a complex with only one H_2 ligand might be important mechanistically. To form a cluster, one phosphine must be lost from such an intermediate, and we suggest three possible mechanistic pathways for this. In pathway A, simple loss of P^iPr_3 from the intermediate dihydrogen complex generates a low-coordinate cationic $\{Rh(P^iPr_3)H_x\}^+$ fragment that is stabilized by fluorobenzene to give **3** (and subsequently **4**). Although these species are observed by NMR spectroscopy, self-assembly of six cationic fragments such as **3** would be unlikely due to charge repulsion. Consistent with this, cluster was not observed to form when pure samples of **3** or **4** were heated at 313 K under H_2. Complexes **3** and **4**, at least in pure form, thus represent mechanistic dead-ends in cluster formation.

The second pathway (B) involves elimination of $[HP^iPr_3]^+$ (as observed in the reaction), possibly through heterolytic H_2 cleavage of coordinated dihydrogen.[85] We have previously discussed this possibility,[39] and examples where such a process is suggested to occur in other cationic dihydrogen complexes exist.[86] This would afford a reactive *neutral monophosphine* $\{Rh(P^iPr_3)H_x\}$ fragment that could then self-assemble to give a neutral cluster. Subsequent oxidation, or more likely protonation by either $[HP^iPr_3]^+$ ($pK_a = 9.0$) or HF formed from the hydrido-defluorination of fluorobenzene in the reaction mixture, would afford the observed dicationic cluster (eq 1, Scheme 8). We have yet to test whether a low-coordinate *neutral* $\{Rh(PR_3)H_x\}$ fragment is a viable intermediate in cluster buildup because suitable synthetic routes to such monophosphine complexes have not yet been developed. A third alternative is the combination of four neutral and two cationic fragments, pathway C. This would afford a cluster directly. One would expect that a neutral $\{Rh(PR_3)H_x\}$ fragment would dimerize at the very least by hydride bridging,[58] and thus cluster condensation could result from addition of "$[Rh(PR_3)H_x]_2$" to $[RhH_2(P^iPr_3)(\eta^6\text{-}C_6H_5X)]$-$[BAr^F_4]$ (X = F (**3**), H (**4**)) to afford a cationic trimetallic species that could then itself dimerize (eq 2, Scheme 8). A related self-assembly process is suggested to occur in the formation of $W_6(C^iPr)(O^iPr)_{12}H_5$ from hydrogenolysis of $W_2(^iBu)_2(O^iPr)_4$, where reactive species such as "$W_2H_2(O^iPr)_4$" are implicated to combine to form "$W_4H_4(O^iPr)_4$" and subsequently associate with $W_2(^iBu)_2(O^iPr)_4$.[22] Related to the loss of $[HPR_3]^+$ as a driver to cluster formation, triflic acid-promoted loss of phosphine has been reported to encourage the formation of $[Pt_6(\mu\text{-}P^tBu_2)_4(CO)_6][OTf]_2$ from the trimetallic precursor $Pt_3(\mu\text{-}P^tBu_2)_3H(CO)_2$.[87]

Repeating the reaction in the presence of a 2-fold excess of $[HP^iPr_3][BAr^F_4]$ completely inhibited cluster formation, showing

that once a significant amount of protonated phosphine has built up in the reaction, cluster formation will cease. This observation is consistent with the apparent equilibrium concentration of $[Rh(P^iPr_3)_2(H)_2(\eta^2\text{-}H_2)][BAr^F_4]$ observed at the end of the reaction, and the idea that repressurizing the reaction with H_2 does not afford more cluster. This inhibition likely comes from a back reaction (protonation and coordination of phosphine) between $[HP^iPr_3][BAr^F_4]$ and a mono-phosphine intermediate involved in cluster buildup.

Although the order of all these possible events discussed, and the actual species involved, needs further clarification before a complete mechanistic picture of the cluster self-assembly can be determined, that the clusters are reproducibly isolated in a good yield ($\sim$30–40%) and are of excellent purity shows that whatever self-assembly mechanisms are operating are experimentally robust. This is an important consideration if the chemistry of these cluster species is to be developed.

Conclusions

The synthesis and characterization of octahedral rhodium cluster complexes under conditions that favor kinetically controlled cluster products has been described: $[Rh_6(PR_3)_6H_{12}]$-$[BAr^F_4]_2$ ($PR_3 = P^iPr_3$, PCy_3; $BAr^F_4 = [B\{C_6H_3(CF_3)_2\}_4]^-$). These clusters are unique in that they have structures that are exactly like those of early transition metal clusters that have edge-bridging π-donor ligands rather than those expected for a late transition metal. These clusters reversibly take up two molecules of dihydrogen to afford clusters that have 16 hydrogens surrounding the metal core. This uptake of H_2 is a consequence of two low-lying unoccupied molecular orbitals that readily accept two electron pairs (or two mole equivalents of H_2). The reversible uptake of dihydrogen is of clear relevance to applications in hydrogen storage, and the drivers behind the reversible storage of large amounts of H_2 ($>$6% by mass for mobile applications) have been described extensively and will not be repeated here.[33] The current best molecular materials are those based around metal–organic frameworks (MOFs),[34] which can reach storage efficiencies of 2.5% at 77 K.[88] Based on the cluster dication core, complex **1a** can store a modest $\sim$0.25% of H_2 at room temperature for the 12-hydride to 16-hydride process, and in terms of the volume of H_2 uptake, **1a** can reversibly take up $\sim$20 times its volume of H_2. Clearly, they do not make suitable candidates for hydrogen storage for mobile applications. However, their well-defined molecular nature that can be probed by NMR, X-ray crystallography, and mass spectrometry as well as DFT calculations means that they make excellent models for reversible hydrogen attachment on a metal surface. Moreover, the ease of filling and emptying the frontier molecular orbitals with electrons (in this case from H_2) without significant structural change suggests that these clusters should present interesting electrochemistry and magnetic behavior, especially when linked to the reversible uptake of H_2 and the extremely high hydride count of the clusters. These aspects, and ways of increasing the hydrogen storage capacity of these clusters by "unlocking" the remaining 12 hydride ligands that surround the metal core, must be future goals associated with this work.

(85) Kubas, G. *Adv. Inorg. Chem.* **2004**, *56*.
(86) Chin, B.; Lough, A. J.; Morris, R. H.; Schweitzer, C. T.; Dagostino, C. *Inorg. Chem.* **1994**, *33*, 6278–6288. Yi, C. S.; Lee, D. W.; He, Z.; Rheingold, A. L.; Lam, K.-C.; Concolino, T. E. *Organometallics* **2000**, *19*, 2909.
(87) de Biani, F. F.; Lenco, A.; Laschi, F.; Leoni, P.; Marchetti, F.; Marchetti, L.; Mealli, C.; Zanello, P. *J. Am. Chem. Soc.* **2005**, *127*, 3076–3089.
(88) Chen, B. L.; Ockwig, N. W.; Millward, A. R.; Contreras, D. S.; Yaghi, O. M. *Angew. Chem., Int. Ed.* **2005**, *44*, 4745–4749.

Experimental Section

General. All manipulations were performed under an inert atmosphere of argon, using standard Schlenk line and glovebox techniques. Glassware was dried in an oven at 130 °C overnight and flamed with a blow torch, under vacuum, three times before use. C_6H_5F was distilled from CaH_2. CH_2Cl_2, pentane, and hexane were purified using an MBraun solvent purification system. CD_2Cl_2 was distilled under vacuum from CaH_2. $[(Cy_3P)_2Rh(nbd)][1-H-closo-CB_{11}Me_{11}]$, $[(Cy_3P)_2Rh(nbd)]-[BArF_4]$, and $[(^iPr_3P)_2Rh(nbd)][BArF_4]$ were prepared by the published route[39] using $Ag[closo-1-H-CB_{11}Me_{11}]$,[40] $K[BArF_4]$,[89] and $^iPr_3P$ or PCy_3. $[Rh(binor-S)(P^iPr_3)][BArF_4]$ was synthesized by the published procedure.[81]

NMR Spectroscopy. ^1H and ^{31}P NMR spectra were recorded on a Bruker Avance 400 MHz FT-NMR spectrometer. Residual protio solvent was used as reference for ^1H NMR spectra (CD_2Cl_2: $\delta = 5.33$). ^{31}P NMR spectra were referenced against 85% H_3PO_4 (external). ^1H NMR spectra in fluorobenzene were referenced to the solvent signal, the position of which was determined using an external sample of TMS. For samples run in protio-fluorobenzene (reaction monitoring experiments), shimming was performed by optimization of line shapes obtained by visual inspection of a real-time Fourier-transformed FID. Coupling constants are quoted in hertz. ^1H NMR spectra were recorded using long delays between pulses (>5 s) to avoid saturation. T_1 measurements were made using the standard inversion−recovery−delay method ($180°−\tau−90°$). PGSE diffusion data were collected at 294 K in 5-mm NMR tubes using the previously outlined method,[63] measuring integrated resonances of the PR_3 groups in the ^1H NMR spectrum. The diffusion coefficient was calculated from the slope of the regression line of the plot $\{\ln(I/I_0)$ vs $G^2\}$.

Mass Spectrometry. ESI-MS data were collected on a Waters Micromass Q-Tof micromass spectrometer in positive-ion mode. Samples were infused by means of a syringe pump at 5 μL min^{-1}. Solutions were made up in an inert-atmosphere glovebox using dry CH_2Cl_2. Capillary voltage was set to 2900 V. To minimize fragmentation of the parent ion, the cone voltage was set to 10 V, and source and desolvation gas temperatures were both set to 30 °C. Theoretical isotope patterns were calculated using Matthew Monroe's Molecular Weight Calculator (http://jjorg.chem.unc.edu/personal/monroe/mwtwin.html).

Computational Details. Calculations were carried out using the ADF code version 2004.1.[90] Vosko, Wilk, and Nusair's local functional was employed with the Becke 88 and the Perdew 86 nonlocal exchange and correlation gradient corrections. The basis sets used were uncontracted triple-ζ Slater-type orbitals (STOs). Hydrogen and phosphorus were given extra polarization functions (2p on H and 4d on P).[91] The cores of atoms were frozen, P up to the 2p level and Rh up to 4p. Scalar ZORA relativistic corrections were used. Calculations for $[Rh_6(PH_3)_6H_{16}]^{2+}$ with 16 hydrides on the octahedral Rh_6 surface result in a final energy of −168.18 eV. Putting one hydride ligand interstitial lowers this energy to −169.68 eV, a difference of 1.5 eV (145 kJ mol^{-1}). The dissociation energy of the two H_2 molecules from the H_{16} cluster, i.e., the SCF energy difference between $[Rh_6H_{12}(PH_3)_6]^{2+} + 2H_2$ and $[Rh_6H_{16}(PH_3)_6]^{2+}$, is calculated as 151 kJ mol^{-1}, with the 16-hydride cluster being the more stable. In addition to full optimizations of both structures, $[Rh_6H_{12}(PH_3)_6]^{2+}$ was also optimized with the $Rh_6H_{12}P_6$ core constrained to octahedral symmetry. Coordinates for the calculated structures have been published as Supporting Information previously.[37]

(89) Buschmann, W. E.; Miller, J. S. *Inorg. Synth.* **2002**, *33*, 85.
(90) Velde, G. T.; Bickelhaupt, F. M.; Gisbergen, S. J. A. V.; Guerra, C. F.; Baerends, E. J.; Snijders, J. G. *J. Comput. Chem.* **2001**, *22*, 931. Guerra, C. F.; Snijders, J. G.; Velde, G. T.; Baerends, E. J. *Theor. Chem. Acc.* **1998**, *99*, 391. ADF, 2004.0 ed.; SCM, Theoretical Chemistry, Vrije Universiteit: Amsterdam, The Netherlands, 2004 (http://www.scm.com).
(91) Vosko, S. H.; Wilk, L.; Nusair, M. *Can. J. Phys.* **1980**, *58*, 1200−1211. Perdew, J. P. *Phys. Rev. B* **1986**, *33*, 8822−8824. Becke, A. D. *Phys. Rev. A* **1988**, *38*, 3098−3100.

$[Rh_6(P^iPr_3)_6H_{12}][BArF_4]_2$ (1a). In a typical experiment, a solution of $[Rh(nbd)(P^iPr_3)_2]$ (200 mg, 0.145 mmol) in fluorobenzene (10 mL) in a J. Young tube was hydrogenated (ca. 4 atm of H_2) by freezing a solution to 77 K, placing the tube under 1 atm of H_2, sealing the tube, and warming to room temperature (298/77 ~ 4) and stirred at 40 °C under ca. 4 atm of H_2 for 5 days. Pentane (50 cm^3) was added, and the mixture was crystallized at −18 °C overnight. The material that resulted was crystallized in the same manner an additional two times. The sample was dissolved in fluorobenzene, and 1-hexene was added to ensure that only $[Rh_6(P^iPr_3)_6H_{12}][BArF_4]_2$ (and none of the 16-hydride species) was present. After 24 h, the solution was layered with hexanes, and slow diffusion gave $[Rh_6(P^iPr_3)_6H_{12}][BArF_4]_2$ as a deep red crystalline solid (25 mg, 31%).

^1H NMR (400 MHz, CD_2Cl_2): δ 7.71 (m, 16H, BArF$_4$), 7.55 (m, 8H, BArF$_4$), 2.32 (m, 18H, PCH), 1.23 (m, 108H, CH$_3$), −25.44 (s, fwhm = 46 Hz, 12H, Rh−H). ^{31}P NMR (162 MHz, CD_2Cl_2): δ 106.2 [d, J(RhP) = 104 Hz]. Selected low-temperature ^1H NMR data: at 250 K, δ −25.44 (s, fwhm 55 Hz); at 200 K, δ −19.03 (s, fwhm 76 Hz, T_1 = 320 ms). ^{13}C NMR (162 MHz, CD_2Cl_2): δ 29.92 (br, fwhm 30 Hz, PCH), δ 20.53 (s, CH$_3$). ESI-MS (CH_2Cl_2): calcd for $[P_6Rh_6C_{54}H_{138}]^{2+}$, 795.2; obsd 795.1. Elemental analysis: $C_{118}H_{162}F_{48}B_2P_6Rh_6 \cdot C_6H_5F$ requires C 43.63, H 4.93; found C 43.48, H 4.86.

$[Rh_6(P^iPr_3)_6H_{16}][BArF_4]_2$ (1b). A solution of **1a** (5 mg) in dichloromethane (0.5 cm^3) was placed under a hydrogen atmosphere (4 atm) for 2 min in a J. Young NMR tube by freezing a solution to 77 K, placing the tube under 1 atm of H_2, sealing the tube, and warming to room temperature (298/77 ~ 4). Alternatively, placing the sample under 1 atm of H_2 effects conversion in 10 min. Conversion to $[Rh_6(P^iPr_3)_6H_{16}]-[BArF_4]_2$ (**1b**) was quantitative by NMR spectroscopy. Although crystalline material was readily available by recrystallization from fluorobenzene/pentane under a H_2 atmosphere (as checked by ESI-MS and NMR), the crystals that resulted always gave diffraction patterns that were indicative of long-range disorder in the solid state. Other solvent/anion combinations did not produce better quality crystals. Alternatively, finely crystalline or finely powdered **1a** (~5 mg) was treated with H_2 (~4 atm) in a J. Young tube for 10 h, resulting in quantitative conversion (by ESI-MS and NMR) to **1b**.

^1H NMR (400 MHz, CD_2Cl_2, 298 K under 1 atm of H_2; free H_2 observed at δ ~4.6 as a sharp singlet): δ 7.71 (m, 16H, BArF$_4$), 7.55 (m, 8H, BArF$_4$), 2.27 (m, 18H, PCH), 1.24 [dd, J(PH) = 15.4 Hz, J(HH) = 7.1 Hz, 108H, CH$_3$], −21.46 (s, fwhm 40 Hz, 15H, Rh−H), −29.81 (br s, fwhm 200 Hz, 1H, Rh−H). $^{31}P\{^1H\}$ NMR (162 MHz, CD_2Cl_2): δ 109.2 [d, J(RhP) = 140 Hz]. Selected low-temperature ^1H NMR data: at 200 K, δ −16.5 to −25.9 (at least eight signals, all signals show $T_1 \approx 330$ ms), −29.3 (T_1 = 430 ms), total integral over hydride region = 12.9 relative to ^iPr groups; the peak at δ −29.3 (assigned as the interstitial hydride in the 298 K spectrum) integrates to ~1H in both room-temperature and low-temperature spectra. ESI-MS (CH_2Cl_2): calcd for $[P_6Rh_6C_{54}H_{142}]^{2+}$, 797.2; obsd, 797.3. Elemental analysis was not obtained due to loss of H_2 under vacuum. Characterization by NMR and ESI-MS is unequivocal.

Synthesis of $[Rh_6(PCy_3)_6H_{12}][BArF_4]_2$ (2a). In a typical experiment, a solution of $[Rh(nbd)(PCy_3)_2][BArF_4]$ (500 mg, 0.31 mmol) in fluorobenzene (20 mL) in a J. Young tube was hydrogenated (ca. 4 atm of H_2) by freezing a solution to 77 K, placing the tube under 1 atm of H_2, sealing the tube, and warming to room temperature (298/77 ~ 4 atm) and held at 50 °C under ca. 4 atm of H_2 for 5 days. Pentane (80 cm^3) was added, and the mixture was crystallized at 5 °C overnight. The residue was dissolved in dichloromethane (5 mL), 1-hexene (0.5 cm^3) was added, and the mixture was heated to 40 °C for 40 h to effect conversion to the 12-hydride species. The solvent was removed in vacuo, and the dark material was repeatedly crystallized from dichloromethane/toluene until negligible colorless material ($[HPCy_3][BArF_4]$) cocrystallized. The solid was dissolved in dichloromethane, and slow diffusion of toluene into the solution gave $[Rh_6(PCy_3)_6H_{12}][BArF_4]_2$ as

a deep red solid (84 mg, 40%). NMR and ESI data of the resulting crystals were unequivocal in the characterization as the 12-hydride species.

¹H NMR (400 MHz, CD₂Cl₂, 298 K): δ 7.71 (m, 16H, BAr$^F_4$), 7.55 (m, 8H, BAr$^F_4$), 0.8−2.5 (m, 198H, PCy₃), −27.20 (br s, fwhm 230 Hz, 9H, Rh−H), −28.9 (br s, fwhm 330 Hz, 3H, Rh−H). Selected variable-temperature ¹H NMR data: at 330 K, δ −21.7 (12H); at 250 K, δ −21.7 (9H), −25.2 (3H); at 200 K, δ −19.52 (9H, T_1 = 890 ms), −21.94 (3 H, T_1 = 890 ms). ³¹P{¹H} (162 MHz, CD₂Cl₂, 298 K): δ 91.9 [d br, J(RhP) = 102Hz]; at 200 K, δ 88.2 [d, J(RhP) = 105 Hz]; at 348 K, 100.4 (vbr s, fwhm 200 Hz]. ESI-MS (CH₂Cl₂): calcd for [P₆Rh₆C₁₀₈H₂₁₀]²⁺, 1155.5; obsd, 1155.7. Elemental analysis: C₁₇₃H₂₃₄B₂-F₄₈P₆Rh₆·1.5CH₂Cl₂ requires C 50.02, H 5.73; found C 49.95, H 5.49. Solvent of crystallization (CH₂Cl₂) is found in the solid-state structure.

Synthesis of [Rh₆(PCy₃)₆H₁₆][BAr$^F_4$]₂ (2b). A solution of [Rh₆-(PCy₃)₆H₁₂][BAr$^F_4$]₂ (5 mg) in CD₂Cl₂ (0.5 mL) was shaken under a hydrogen atmosphere (4 atm) for 2 min in a J. Young NMR tube. Alternatively, placing a solution of **2a** under 1 atm of H₂ effects conversion in 10 min. Conversion to [Rh₆(PCy₃)₆H₁₆][BAr$^F_4$]₂ (**2b**) was quantitative by NMR spectroscopy. The solution was layered with pentane, and slow diffusion gave [Rh₆(PCy₃)₆H₁₆][BAr$^F_4$]₂ as a deep red solid (4.5 mg, 90%). The crystalline material that resulted gave a poor-quality refinement (R_1 > 9%). Other solvent combinations did not produce better quality crystals. Use of the weakly coordinating anion [1-H-*closo*-CB₁₁Me₁₁]⁻ in place of [BAr$^F_4$]⁻ (starting from [(Cy₃P)₂-Rh(nbd)][1-H-*closo*-CB₁₁Me₁₁]) gave reasonable quality crystals (R_1 < 5%). The structures of both cluster cores are similar, and the hydrogen atoms could not be reliably located in either. Alternatively, finely crystalline or finely powdered **2a** (∼5 mg) was treated with H₂ (∼4 atm) for 10 h in a J. Young tube, resulting in quantitative conversion (by ESI-MS and NMR) to **2b**.

¹H NMR (400 MHz, CD₂Cl₂, 298 K under 1 atm of H₂; free H₂ is observed at δ ∼4.6): δ 7.71 (m, 16H, BAr$^F_4$), 7.55 (m, 8H, BAr$^F_4$), 1.0−2.4 (m, 198H, PCy₃), −21.59 (br s, fwhm 190 Hz, 15H, Rh−H), −28.37 (br s, fwhm 390 Hz, 1H, Rh−H). Selected low-temperature ¹H NMR data: at 200 K, δ −26.71 (T_1 = 940 ms), others (all ∼1100 ms); total integral over hydride region = 12.3 H relative to Cy groups. ³¹P{¹H} NMR (162 MHz, CD₂Cl₂, 298 K): δ 107.4 (br s, fwhm 1100 Hz, 2P), 89.0 (br s, fwhm 900 Hz, 4 P). ESI-MS (CH₂Cl₂): calcd for [P₆Rh₆C₁₀₈H₂₁₄]²⁺, 1157.5; obsd, 1157.8. Elemental analysis was not obtained due to loss of H₂ under vacuum. Characterization by NMR and ESI-MS is unequivocal.

[Rh(H)₂(C₆H₅F)(P^{i}Pr₃)][BAr$^F_4$]₂ (3). A solution of [(binor-*S*)Rh-(P^{i}Pr₃)][BAr$^F_4$] (5 mg) and fluorobenzene (0.5 mL) was placed under 4 atm of of dihydrogen (see **1a** for details). The solution was shaken and allowed to stand for 15 min, resulting in quantitative conversion to **3**, as determined by in situ ¹H and ³¹P NMR spectroscopy. Compound **3** could not be isolated in solid form, and so characterization rests on spectroscopic data alone.

¹H NMR (400.1 MHz, C₆H₅F): δ 6.32 (m, 2H, C₆H₅F), 6.18 (m, 2H, C₆H₅F), 5.82 (m, 1H, C₆H₅F), 1.54 [apparent octet, J(HH) ≈ J(PH) ≈ 7.5 Hz, 3H, PCH], 0.74 [dd, J(PH) = 16.2 Hz, J(HH) = 7.1 Hz, 18H, CH₃], −14.98 [ddd, J(RhH) = 29.1 Hz, J(PH) = 23.2 Hz, J(FH) = 1.6 Hz, 2H, Rh−H]. ³¹P NMR (162.0 MHz, C₆H₅F): δ 95.45 [dd, J(RhP) = 141 Hz, J(FP) = 1.7 Hz]. ¹⁹F NMR (376.5 MHz, C₆H₅F): δ −109.8 (br s). In ³¹P{¹H-selective} experiments, *only* the isopropyl alkyl phosphine protons (δ 2.3−1.2 ppm) lead to a ³¹P{¹H-selective} NMR spectrum that is a doublet of triplets [J(RhP) = 141 Hz, J(HP)

= 23 Hz], indicating a hydride count of two (the small ¹⁹F coupling is not resolved in this experiment).

[Rh(P^{i}Pr₃)(H₂)(η^6-C₆H₆)][BAr$^F_4$] (4). A solution of [(binor-*S*)Rh-(P^{i}Pr₃)][BAr$^F_4$] (5 mg) and benzene (50 μL) in CD₂Cl₂ (0.5 mL) was placed under 4 atm of dihydrogen in a J. Young NMR tube. The solution was shaken and allowed to stand for 15 min, resulting in quantitative conversion to **5**, as determined by in situ ¹H and ³¹P NMR spectroscopy. The NMR data for the cation are essentially the same as those reported for the [PF₆]⁻ salt. [82]

Selected ¹H NMR (400 MHz, CD₂Cl₂): δ 6.77 (s, 6H, C₆H₆), 1.94−2.07 (m, 3H, PCH), 1.12 [dd, J(HH) = 16.0 Hz, J(PH) = 7.1 Hz, 18H, CH₃], −14.54 [dd, J(PH) = 27.7 Hz, J(RhH) = 23.6 Hz, 2H, Rh−H]. ³¹P{¹H} NMR (162 MHz, CD₂Cl₂): δ 96.3 [d, J(RhP) = 142 Hz].

X-ray Crystallography. Intensity data for **1a**, **2a**, and **2b** were collected at 150 K on a Nonius KappaCCD diffractometer equipped with a low-temperature device, using graphite-monochromated Mo Kα radiation (λ = 0.71073 Å). Data were processed using the supplied Nonius software. For **2a**, a symmetry-related (multiscan) absorption correction was employed. Crystal parameters and details on data collection, solution, and refinement for the complexes are provided in Table 1. Structure solution, followed by full-matrix least squares refinement, was performed using the WinGX-1.70 suite of programs throughout. For **1a** and **2a**, all 12 hydrogen atoms were found in bridging positions around the Rh₆ core and could be refined freely, whereas in **2b** only 5 out of 16 hydrogen atoms could be found and refined reliably in the final stages of the refinement. In **1a**, a few of the CF₃ groups of the [BAr$^F_4$]⁻ anion show rotational disorder in the ratio 40:60. Compound **1a** co-crystallizes with one molecule of fluorobenzene solvent, which is located around a center of inversion and shows symmetry-related disorder of the F atom. In **2a**, co-crystallization occurs with one toluene molecule and dichloromethane solvent that refines best to a partial occupancy of 2.75. All the solvent molecules show some kind of disorder, and most of them are only partly occupied within the lattice. The toluene molecules share their site with CH₂Cl₂ molecules and therefore had to be restrained and refined isotropically. Crystallographic data files have been deposited with the Cambridge Crystallographic Data Service (CCDC, 12 Union Rd., Cambridge CB2 1EZ, UK; tel. (+44) 1223-336-408; fax (+44) 1223-336-033, E-mail deposit@ccdc.cam.ac.uk) under the following codes: **1a**, 603489; **2a**, 603490; and **2b**, 275849.

Supporting Information Available: X-ray crystallographic data for **1a**, **2a**, and **2b**; low-temperature (250 K) ¹³C{¹H} NMR spectrum of **2a**; room-temperature (298 K) ¹³C{¹H} NMR spectrum of **1a**; ¹H and ³¹P{¹H selective} NMR data for **3**; ³¹P-{¹H} NMR spectra over 5 days for the cluster formation reaction; synthesis, NMR, and X-ray crystallographic data for **5**. CIF files for all the crystal structures reported in this paper. This material is available free of charge via the Internet at http://pubs.acs.org.

JA0604663